

The Catolé do Rocha Batholith (RN-PB): A reduced A₂-type granitic magmatism in the Rio Piranhas-Seridó Domain, Borborema Province, Northeastern of Brazil

O Batólito Catolé do Rocha (RN-PB): Um magmatismo granítico do tipo-A₂, reduzido no Domínio Rio Piranhas-Seridó, Província Borborema, Nordeste do Brasil

Robson Rafael de Oliveira^{1,2} , Frederico Castro Jobim Vilalva^{1,3} , Adriana Alves⁴ , Vladimir Cruz de Medeiros⁵ , Clarissa de Aguiar Dalan¹ 

¹Universidade Federal do Rio Grande do Norte - UFRN, Programa de Pós-Graduação em Geodinâmica e Geofísica, Avenida Senador Salgado Filho, 3000, Caixa Postal 1596, Lagoa Nova, CEP 59078-970, Natal, RN, BR (robson.oliveira@ifrn.edu.br, frederico@geologia.ufrn.br, clarissa.dalan@gmail.com)

²Instituto Federal de Educação, Ciência e Tecnologia do Rio Grande do Norte - IFRN, Parelhas, RN, BR.

³UFRN, Departamento de Geologia, Natal, RN, BR.

⁴Universidade de São Paulo - USP, Instituto de Geociências, São Paulo, SP, BR (adrianaalves@usp.br)

⁵Serviço Geológico do Brasil - CPRM, Superintendência de Recife, Recife, PE, BR (vladimir.medeiros@cprm.gov.br)

Received on January 30, 2020; accepted on August 19, 2020

Abstract

The Catolé do Rocha Batholith, situated in the Rio Piranhas-Seridó Domain of the Borborema Province (Northeastern (NE) Brazil), is an important example of the post-collisional Ediacaran magmatism that affected this region. It includes metaluminous to slightly peraluminous sienogranite and quartz syenite, basic-intermediate rocks and minor microgranite dykes; the whole set is intrusive in the Paleoproterozoic basement. This batholith has been interpreted as a member of the high-K calc-alkaline magmatic suite with chemical affinities akin to the Caledonian I-type granites. However, there are many lithochemical evidence associating the batholith to the A-type magmas. The granites are alkali-calcic to alkaline, have ferroan character, significant concentrations of large-ion lithophile elements (LILE) and high-field-strength elements (HFSE) and relative enrichment of light rare earth elements (LREE) than heavy rare earth elements (HREE). Their chemical signatures agree with a post-collisional A₂-type setting. Geothermobarometric estimates provide crystallization at pressures of 4.6 – 6.3 kbar (ca. 16 – 24 km in depth) and temperatures in the range of 950 – 750°C, under low oxygen fugacity conditions ($-4 < \Delta_{QFM} < -1$). Geochemical data and distinct redox crystallization conditions for the felsic and basic-intermediate rocks suggest they represent distinct magma batches, with local mixing and mingling features. The origin of the batholith seems to be related to enriched (metasomatized) sources, with differentiation controlled mostly by fractional crystallization processes.

Keywords: Catolé do Rocha batholith; A-type granites; Lithochemistry; Crystallization conditions; Borborema Province.

Resumo

O Batólito Catolé do Rocha, situado no Domínio Rio Piranhas-Seridó da Província de Borborema (Nordeste (NE) do Brasil), é um importante representante do magmatismo ediacarano pós-collisional que acometeu essa região. Ele inclui sienogranitos e quartzo sienitos metaluminosos a ligeiramente peraluminosos, rochas básico-intermediárias e, subordinadamente, diques e/ou bolsões de microgranitos menores. Esse batólito é tido como representante da suíte cálcio-alcalina de alto K, que inclui principalmente granitos de afinidade química próxima aos de tipo-I caledonianos. Contudo, são diversas as evidências litoquímicas que aproximam o batólito aos magmas de tipo-A. As rochas graníticas são álcali-cálcicas a alcalinas, possuem caráter *ferroano*, concentrações significativas de elementos litófilos de raio grande (LILE) e de alto potencial iônico (HFSE) e enriquecimento de terras-raras leves (LREE) sobre pesados (HREE). Suas assinaturas químicas permitem classificá-los como granitos de tipo-A₂ pós-collisionais. Estimativas geotermobarométricas apontam cristalização sob pressões de 4,6 – 6,3 kbar (~16 – 24 km de profundidade) e temperaturas entre 950 – 750°C, em condições de baixa fugacidade de oxigênio ($-4 < \Delta_{QFM} < -1$). Evidências químicas e distintas condições redox estimadas para os granitos e rochas básicas-intermediárias do batólito sugerem que se trata de magmas distintos, com misturas do tipo *mixing* e *mingling* locais. A origem do batólito parece estar relacionada a fontes enriquecidas (metassomatizadas), com diferenciação controlada principalmente por processos de cristalização fracionada.

Palavras-chave: Batólito Catolé do Rocha; Granitos tipo-A; Litoquímica; Condições de cristalização; Província Borborema.

INTRODUCTION

One of the most remarkable features in the Borborema Province (Northeastern (NE) Brazil) is the occurrence of a voluminous and extensive granitic syn- to late-orogenic magmatism formed at the end of the Brasiliano Cycle (~580 Ma). In the region between the Rio Grande do Norte and the northern Paraíba states, this magmatism encompasses ca. 80 plutons with distinct mineralogical, petrographic, lithochemical, geochronological and isotopic characteristics that were grouped into six magmatic suites by Nascimento et al. (2015): Shoshonitic, Porphyritic High-K Calc-Alkaline (CALCKP), Equigranular High-K Calc-Alkaline, Calc-Alkaline, Alkaline (ALK) and Charnockitic. The CALCKP Suite stands out in terms of volume and exposed area, with the Catolé do Rocha Batholith (CRB) as one of its largest bodies. Located near the homonymous city in the Paraíba state and intrusive into the paleoproterozoic rocks of the Rio Piranhas-Seridó Domain (PSD), this batholith of ca. 900 km² is composed of a main syenogranite pluton and three satellite stocks, as well as minor occurrences of basic-intermediate rocks, dykes and/or pockets of microgranites (Medeiros et al., 2007).

Previous geochemical and petrographic studies have included the CRB in the CALCKP Suite (Nascimento et al., 2015; Campos et al., 2016) with geochemical characteristics akin to post-collisional I-type granites (Caledonian I-type *sensu* Pitcher, 1983, 1997; cf. Frost et al., 2001; Castro, 2019), formed in oxidized crystallization environments. However, as pointed out by Campos et al. (2016), the Catolé do Rocha granites show a contrasting and more alkaline signature that are typical of A-type magmas crystallized under more reducing conditions (Whalen et al., 1987; Bonin, 2007; Dall'Agnol and Oliveira, 2007).

This work re-evaluates the geochemical and granite typological classifications of the CRB based on new petrographic, lithochemical and mineral chemistry data. We will show that the batholith can be classified as “reduced” A₂-type granites from the ALK Suite (cf. Dalan et al., 2019). Furthermore, the intensive crystallization parameters (P, T, f_{O₂}) will also be refined. As a final goal, we expect to contribute to a better understanding of the formation and geological implications of the Ediacaran plutonism in the PSD.

GEOLOGICAL BACKGROUND

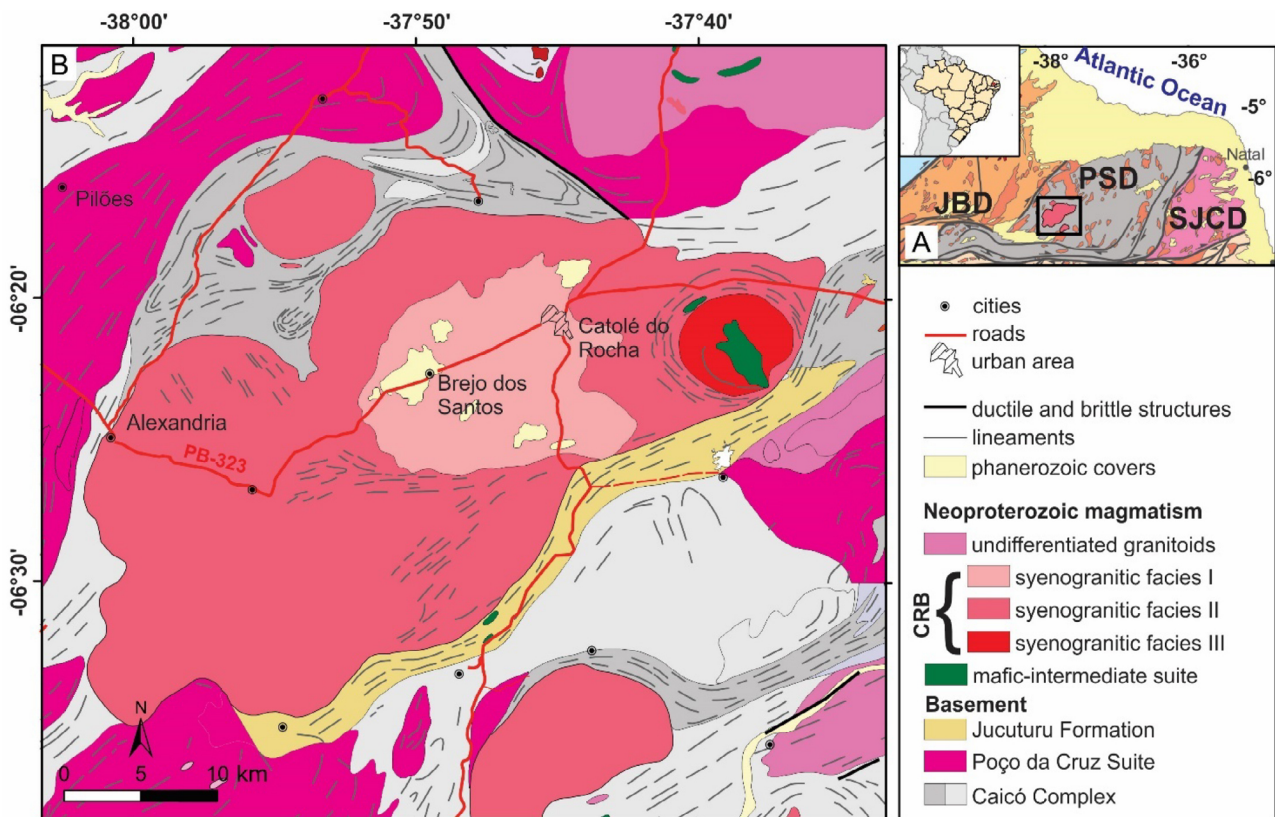
The Borborema is a Precambrian Province of the NE Brazil (Almeida et al., 1981; Brito Neves et al., 2000; Santos et al., 2018) formed by the agglutination of large allochthonous crustal blocks during orogenic events (Jardim de Sá et al., 1992; Jardim de Sá, 1994; Santos, 1996; Santos et al., 2000). Its current configuration includes tectonic domains

that resulted from the diachronic convergence of the West African, Amazonian and São Francisco-Congo cratons during the Brasiliano Cycle (Caby et al., 1991; Jardim de Sá, 1994; Vauchez et al., 1995; Archanjo et al., 2013; Souza et al., 2016; Ferreira et al., 2020), with the generation of shear zones and a large, chemically diverse, granite plutonism (Nascimento et al., 2008, 2015).

In its northernmost portion, the Borborema Province can be divided into three tectonostructural domains called São José do Campestre (to the east), Rio Piranhas-Seridó (central part) and Jaguaribeano (to the west) (Figure 1A). The CRB locates in the western part of the PSD. It is intrusive into Paleoproterozoic basement rocks that include metasupracrustal sequences sectioned by metaplutonic rocks of the Caicó Complex and the Poço da Cruz suite, with ages between 2.25 and 2.17 Ga (Jardim de Sá, 1994; Angelim et al., 2006; Medeiros et al., 2008b; Hollanda et al., 2011; Souza et al., 2007, 2016). Moreover, Cunha et al. (2018) recognized the occurrence of Neoproterozoic biotite-amphibole gneisses of the Jucurutu Formation to the northeast of the batholith. The CRB is composed of syenogranite and quartz syenite, basic-intermediate rocks, as well as dykes and/or microgranite pockets. The syenogranite was dated at 571 ± 3 Ma (U-Pb in zircon) by Medeiros et al. (2007). On structural grounds, the CRB is located near two large shear zones (Figure 1A), the Patos Lineament (to the south) and the Portalegre Shear Zone (to the northwest). Additionally, based on in-depth analysis of regional magnetic data from the PSD, Gonçalves (2009) identified significant magnetic lineaments attributed to deep-seated shear zones, such as the Caicó-Bom Jesus Lineament possibly located in depth below the CRB.

This work focuses on the CRB main body, whose rocks are grouped into three distinct petrographic facies (Figure 1B): Syenogranite I, Syenogranite II and Syenogranite III (or facies I, II and III for the sake of simplicity). These units correspond, respectively, to the Brejo dos Santos, Alexandria and Manicoba facies (Medeiros et al., 2007, 2008b). The Syenogranite I facies includes medium to coarse-grained porphyritic biotite-amphibole syenogranite and leucocratic quartz syenite, with microcline megacrysts up to 3.0 cm long (Figure 2A). Syenogranite II facies is similar to facies I, although with lower amphibole contents and slightly larger microcline megacrysts (Figure 2B). Syenogranite III comprises coarse-grained hololeucocratic to leucocratic biotite syenogranite (Figure 2C).

Microgranular dioritic enclaves occur in all facies. They show rounded or globular shapes, including mingling (Figures 2D and 2E) and mixing/hybridization features (Figure 2D), as well as ellipsoidal biotite-rich layers (rings ?) and schlierens (Figure 2F). Nevertheless, most of the basic and intermediate rocks occurs in the central portion of the Syenogranite III facies (Figure 1B).



PSD: Rio Piranhas Seridó Domain; JBD: Jaguaribeano Domain; SJCD: São José do Campestre Domain.
Source: modified and updated from Medeiros et al. (2008a) and Cunha et al. (2018).

Figure 1. (A) Geological sketch of the northernmost part of the Borborema Province (NE-Brazil), showing the main tectono-structural domains, shear zones and location of the study area. (B) Geological setting of the Catolé do Rocha Batholith intruded in Paleoproterozoic basement rocks.

The outer portions of the batholith are characterized by oriented, stretched potassic feldspar megacrysts (syn to late-tectonic fabric). In turn, magmatic pre-tectonic fabrics include a concentric structure situated at Syenogranite III facies (Figure 1B) and the magmatic alignment of euhedral mafic minerals and potassic feldspar megacrysts and enclaves.

MATERIALS AND METHODS

Representative samples of the CRB granites, basic-intermediate rocks and microgranites were selected for petrographic and chemical (whole-rock and mineral chemistry) studies. Petrographic and textural analysis of selected thin sections were done using transmitted and reflected light petrographic microscopes of the Departamento de Geologia, Universidade Federal do Rio Grande do Norte, following classical petrographic techniques.

Whole-rock composition (major and trace elements) for six samples (two syenogranites and four basic-intermediate

rocks) were obtained by X-ray fluorescence (XRF) at the GeoAnalítica-USP core facility, Instituto de Geociências, Universidade de São Paulo (analytical routines described in Mori et al., 1999). These were added to the litochemical database (18 samples) compiled from Medeiros et al. (2008a, 2008b).

In situ major element compositions of amphibole ($n = 12$) and biotite ($n = 7$) crystals were obtained by energy dispersive spectroscopy (EDS) semiquantitative microanalyses using a EDX-7000/8000 (Oxford Instruments) equipment, coupled to the scanning electronic microscope (SEM), model VEGA3 (TESCAN) of the Laboratório de Caracterização de Minerais e Materiais do Instituto Federal de Educação, Ciência e Tecnologia do Rio Grande do Norte (LACAMM-IFRN/CNAT). Analytical conditions were 20kV for acceleration voltage, 20nA for current, and beam diameter of $1 \mu\text{m}$, with an average acquisition time of 50s. The results were added to the database of Campos et al. (2016) for further geothermobarometric calculations. Additionally, zircon and titanite trace elements

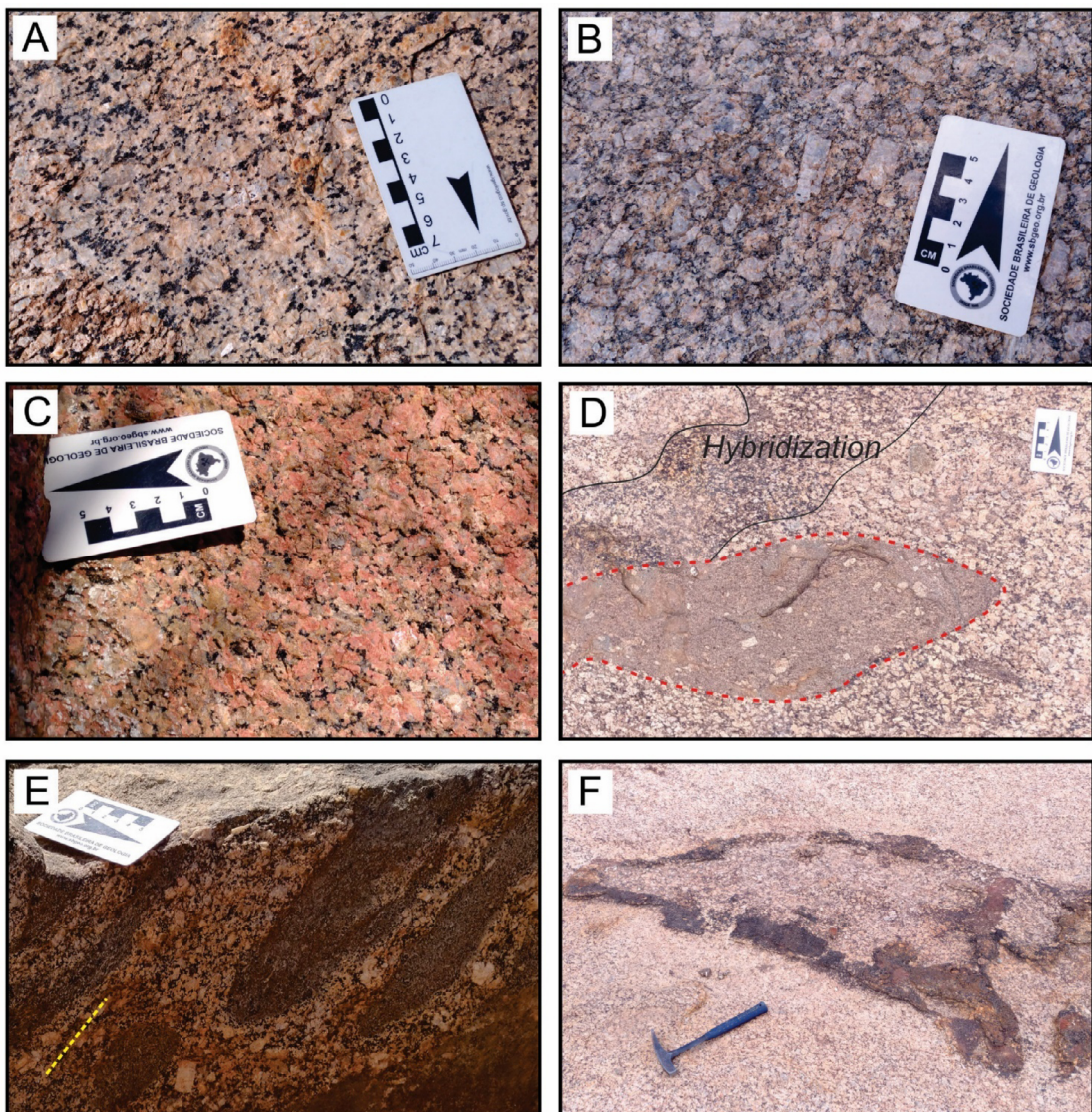


Figure 2. Macroscopic structural and textural aspects of Catolé do Rocha Batholith. (A) Syenogranite of facies I: leucocratic, coarse-grained, inequigranular biotite-amphibole syenogranite with potassic feldspar (red), quartz (grey) and interstitial and oriented biotite and amphibole crystals (black) defining an incipient (magmatic?) foliation. (B) Syenogranite of facies II: leucocratic, coarse-grained, porphyritic biotite syenogranites with potassic feldspar megacrysts (pink) in a quartzo-feldspathic matrix with interstitial biotite ± amphibole (black). (C) Syenogranite of facies III: hololeucocratic, coarse-grained, inequigranular biotite syenogranite, with potassic feldspar (red), quartz (grey) and interstitial biotite (black) biotite. (D) Microgranular mafic enclave (red dashed line) with potassic feldspar xenocrysts hosted in syenogranite of facies I. Note also mafic hybrid portion within the syenogranite suggesting magma mixing processes. (E) Microgranular mafic enclaves with rounded and elliptical shapes, the latter with axis parallel to the magmatic fabric in syenogranites of facies I (yellow dashed line). (F) Metric ellipsoidal (ring?) schlieren hosted in syenogranites of facies I.

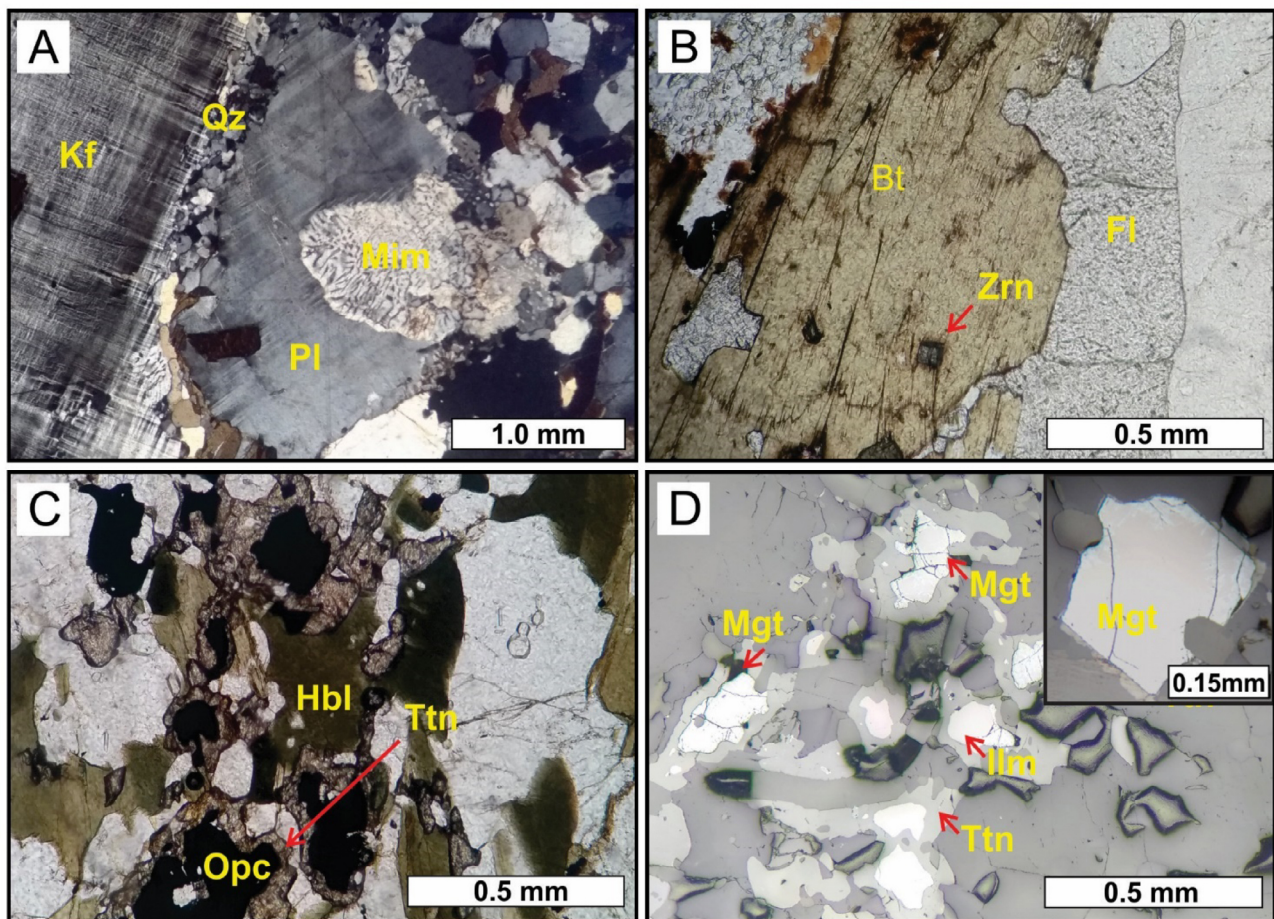
were quantified by laser ablation in the GeoAnalítica-USP LA-ICP-MS facility in selected crystals from the syenogranite I facies. The ablation experiments were performed under an energy fluence of 3.6 J/cm^2 , repetition frequency of 15 Hz and laser diameter of 40 μm . The total acquisition time was 120 s, with integration and dwell time of

1.6 and 25 ms, respectively. NIST-SRM 610 and USGS BIR-1G reference materials were the external standards, and the mean contents (% weight) of CaO (titaniite) and SiO_2 (zircon), obtained for the same sample via EDS, were used as internal standards. Data reduction were performed with the Glitter software (Griffin et al., 2008).

PETROGRAPHIC FEATURES

The batholith consists essentially of syenogranite and subordinate quartz syenite. These are coarse to medium-grained, leucocratic, inequigranular to porphyritic rocks, with potassic feldspar megacrysts up to 3.0 cm. All syenogranite facies have similar mineralogy, with variations in the modal contents of the essential minerals. Facies I contains microcline (40 – 48% modal), oligoclase (An_{22} ; 20 – 23%) and quartz (12 – 25%). Main mafic minerals are biotite (3 – 6%) and hornblende (hastingsite and ferroedenite; 7 – 11%) that eventually are oriented defining an incipient magmatic foliation (Figure 2A). Facies II is composed of microcline (35 – 40%) (Figure 3A), oligoclase (An_{23} ; 19 – 25%) and quartz (18 – 20%), with hornblende

(ferro-pargasite, hastingsite and ferro-edenite; 4 – 6%) and biotite (annite; 6 – 8%) as the mafic phases. Facies III consists of microcline (44 – 56%), sodic oligoclase (An_{17} ; 15 – 20%), quartz (15 – 25%) and biotite (7 – 10%) as the chief mafic mineral (Figure 3B). In all cases, accessory minerals include titanite (1 – 4%), ilmenite \pm titanomagnetite (1 – 2%; Figures 3C and 3D) and fluorite (2%; Figure 3B), as well as minor occurrences of apatite, zircon and allanite. Chlorite, secondary titanite, white mica and carbonates are post-magmatic/hydrothermal phases. Microcline is always perthitic or mesoperthitic and wartlike myrmekites are widespread (Figure 3A). Evidence of superimposed deformation includes deformed, sigmoidal microcline crystals and megacrysts, recrystallized quartz in contact with feldspars (Figure 3A), and undulose extinction in quartz.



Qz: quartz; Kf: potasssic feldspar; Pl: plagioclase; Bt: biotite; Hbl: hornblende; Ttn: titanite; Opc: opaque minerals; Mgt: titanomagnetite; Ilm: ilmenite; Mim: myrmekite.

Figure 3. Microscopic textural aspects of the Catolé do Rocha granites. (A) Millimetric band of (recrystallized?) quartz and myrmekite along the contact between potasssic feldspar and plagioclase crystals, as well as wartlike myrmekites in syenogranite of facies II. (B) Platly biotite crystal with zircon inclusion in contact with interstitial fluorite in syenogranite of facies III. (C) Opaque mineral replaced by secondary titanite (sphenitization), in contact with interstitial hornblende in syenogranite of facies I. (D) Titanomagnetite and ilmenite crystals overgrown by titanite (sphenitization) in syenogranites of facies II. Inset shows euhedral magnetite with borders replaced by martite. Photomicrographs under transmitted (A, B and C) and reflected (D) light with crossed (A) and uncrossed (B, C and D) nicols.

LITHOCHEMICAL FEATURES

Table 1 presents the compositional ranges (major and trace elements) for the CRB, and the compositions of the ALK and CALCKP Ediacaran-Cambrian magmatic suites within the Rio Piranhas-Seridó and São José do Campestre Domains (data compiled from Campos et al., 2000; Nascimento et al.,

2015; Souza et al., 2017). A detailed lithochemical discussion for CRB felsic and basic-intermediate rocks can be found in Medeiros et al. (2008b). Here we present the main aspects that will support our ongoing discussions.

Overall, the batholith has SiO_2 ranging from 62.4 to 75.1 wt.%, enrichment in alkalis ($\text{Na}_2\text{O} + \text{K}_2\text{O} = 8.3 - 10.6\%$) relative to CaO (0.8 – 2.8%), high $\text{K}_2\text{O}/\text{Na}_2\text{O}$ ratios (1.6 – 2.0%)

Table 1. Major and trace element compositional ranges for granites of the Catolé do Rocha Batholith (compiled from Medeiros et al., 2008a, along with our unpublished data) compared to the compositions of the Alkaline and Porphyritic High-K Calc-Alkaline Suites of the Edicaran-Cambrian plutonism in the Rio Piranhas-Seridó and São José do Campestre Domains (data compiled from Campos et al., 2000; Nascimento et al., 2015 and Souza et al., 2017).

Fácies	Syenogranite I	Syenogranite II	Syenogranite III	ALK	CALCKP
Samples (n)	5	5	4	78	71
SiO_2 (wt. %)	62.4 – 70.6 ($\bar{x} = 66.5$)	66.1 – 70.9 ($\bar{x} = 68.5$)	73.9 – 75.1 ($\bar{x} = 74.5$)	67.8 – 76.8 ($\bar{x} = 72.3$)	63.4 – 75.0 ($\bar{x} = 69.2$)
TiO_2	0.3 – 0.7 (0.5)	0.4 – 0.8 (0.6)	0.17 – 0.2 (0.185)	< dl – 0.4 (0.2)	0.1 – 1 (0.55)
Al_2O_3	14.4 – 16.7 (15.55)	13.5 – 15.0 (14.25)	12.4 – 13.6 (13.0)	12.5 – 16.8 (14.65)	12.6 – 17.2 (14.9)
FeOt	3.1 – 5.3 (4.2)	2.9 – 4.5 (7.4)	1.7 – 2.2 (1.95)	0.2 – 2.4 (1.3)	1.0 – 6.6 (3.8)
MnO	0.04 – 0.09 (0.065)	0.04 – 0.06 (0.05)	0.03 – 0.04 (0.035)	< dl – 0.10 (0.05)	0.01 – 0.12 (0.065)
MgO	0.1 – 0.9 (0.5)	0.4 – 0.9 (0.65)	0.19 – 0.2 (0.195)	< dl – 0.6 (0.3)	0.1 – 2.2 (1.15)
CaO	1.4 – 2.8 (2.1)	1.1 – 2.3 (1.7)	0.8 – 0.9 (0.85)	0.2 – 1.4 (0.8)	0.8 – 4.1 (2.45)
Na_2O	3.2 – 3.8 (3.5)	3.0 – 3.6 (3.3)	3.1 – 3.3 (3.2)	2.8 – 5.9 (4.35)	2.9 – 5.6 (4.25)
K_2O	6.2 – 6.8 (6.5)	5.8 – 6.2 (6.0)	5.2 – 6.0 (5.6)	3.1 – 8.4 (5.75)	3.6 – 6.3 (4.95)
P_2O_5	0.03 – 0.2 (0.115)	0.09 – 0.3 (0.195)	0.03 – 0.06 (0.045)	< dl – 0.13 (0.065)	< dl – 0.4 (0.2)
A/CNK	0.91 – 0.98 (0.945)	0.93 – 1.0 (0.965)	1.01 – 1.03 (1.02)	0.88 – 1.15 (1.015)	1.11 – 1.53 (1.32)
A/NK	1.13 – 1.27 (1.2)	1.15 – 1.26 (1.205)	1.15 – 1.17 (1.16)	1.00 – 1.29 (1.145)	0.83 – 1.04 (0.935)
$\text{K}_2\text{O}/\text{Na}_2\text{O}$	1.69 – 1.98 (1.83)	1.73 – 1.95 (1.84)	1.62 – 1.89 (1.755)	0.66 – 2.89 (1.775)	0.84 – 2.14 (1.49)
$\text{Na}_2\text{O} + \text{K}_2\text{O}$	9.5 – 10.6 (10.05)	8.9 – 9.8 (9.35)	8.3 – 9.3 (8.88)	7.8 – 11.7 (9.75)	7.4 – 10.8 (9.1)
Fe^*	0.81 – 0.97 (0.89)	0.83 – 0.89 (0.86)	0.89 – 0.91 (0.90)	0.76 – 1.0 (0.88)	0.61 – 0.93 (0.77)
A.I.	0.79 – 0.89 (0.84)	0.79 – 0.87 (0.83)	0.86 – 0.87 (0.865)	0.76 – 1.00 (0.88)	0.66 – 0.97 (0.815)
Rb (ppm)	160 – 191 (175.5)	128 – 305 (216.6)	242 – 393 (317.5)	27 – 257 (142)	72 – 376 (224)
Sr	109 – 392 (250.5)	167 – 304 (235.5)	95 – 107 (101)	63 – 1937 (1000)	114 – 702 (408)
Ba	576 – 1823 (1199.5)	795 – 1248 (1021.5)	357 – 448 (402.5)	219 – 4594 (2406.5)	338 – 1682 (1010)
Zr	385 – 914 (649.5)	55 – 552 (303.5)	107 – 205 (156)	8 – 322 (165)	22 – 438 (230)
Hf	10 – 21.4 (15.7)	2.1 – 13.6 (7.85)	4.2 – 6.3 (5.25)	< dl – 9 (4.5)	< dl
Nb	15 – 45 (30)	23 – 135 (79)	19 – 249 (134)	3 – 58 (30.5)	4 – 37 (20.5)
Y	27 – 57 (42)	33 – 58 (45.5)	18 – 33 (25.5)	4 – 103 (53.5)	5 – 48 (26.5)
La	137 – 271 (204)	113 – 247 (180)	59 – 69 (62.5)	2 – 145 (73.5)	13 – 182 (97.5)
Ce	258 – 388 (323)	207 – 447 (327)	97 – 138 (117.5)	5 – 254 (129.5)	23 – 307 (165)
Nd	88 – 140 (114)	62 – 136 (99)	33 – 41 (37)	4 – 96 (50)	10 – 86 (48)
Sm	13 – 20 (16.5)	10 – 18 (14)	5 – 6 (5.5)	1 – 19 (10)	0.6 – 12 (6.3)
Eu	1.7 – 3.2 (2.45)	1.4 – 2.1 (1.75)	0.6 – 0.7 (0.65)	0.6 – 1.5 (1.35)	0.1 – 2.2 (1.15)
Gd	7 – 13 (10)	7 – 12 (9.5)	3.4 – 4.3 (3.85)	0.8 – 17 (8.9)	0.5 – 11 (5.75)
Tb	1.1 – 1.8 (1.45)	1.1 – 1.7 (1.4)	0.6 – 0.8 (0.7)	0.07 – 2.8 (1.435)	< dl
Ho	0.9 – 1.8 (1.35)	1.1 – 1.8 (1.45)	0.6 – 0.9 (0.75)	0.1 – 3 (1.55)	0.04 – 0.3 (0.17)
Yb	2.1 – 5.4 (3.75)	2.6 – 4.3 (3.45)	1.8 – 2.9 (2.35)	0.2 – 7.6 (3.9)	0.1 – 3.2 (1.65)
Lu	0.3 – 0.7 (0.5)	0.4 – 0.7 (0.55)	0.3 – 0.5 (0.4)	0.05 – 1.1 (0.575)	0.02 – 0.5 (0.26)
Sc	3 – 8 (5.5)	3 – 6 (4.5)	1 – 1.5 (1.25)	< dl – 5.4 (2.7)	1 – 7 (4)
V	< dl – 37 (18.5)	9 – 31 (20)	5 – 8 (6.5)	1.2 – 47 (24.1)	8 – 53 (30.5)

Continue...

Table 1. Continuation.

Fácies	Syenogranite I	Syenogranite II	Syenogranite III	ALK	CALCKP
Cr	< dl	< dl	< dl	< dl	< dl
Co	0.9 – 6.6 (3.75)	3.7 – 6.8 (5.25)	1.5 – 2.4 (1.95)	0.03 – 3.1 (1.565)	4 – 5 (4.5)
Ni	< dl	< dl	< dl	< dl	< dl
Cu	6 – 11 (8.5)	6 – 14 (10)	3.7 – 7 (5.35)	1 – 30 (15.5)	6 – 30 (18)
Zn	29 – 77 (53)	47 – 68 (57.5)	29 – 38 (33.5)	6 – 23 (14.5)	11 – 65 (38)
Ga	19 – 24 (21.5)	18 – 22 (20)	17 – 19 (18)	< dl – 47 (23.5)	4 – 31 (17.5)
Pb	2.9 – 9 (5.95)	9 – 25 (17)	5 – 39 (22)	< dl	47 – 60 (53.5)
Th	20 – 40 (30)	33 – 56 (45.5)	35 – 48 (41.5)	< dl – 72 (36)	12 – 50 (31)
U	1.2 – 2.1 (1.65)	1.2 – 3.3 (2.2)	3.5 – 6.4 (4.65)	< dl – 5.4 (2.7)	< dl

A/CNK = (molar Al_2O_3)/(CaO + Na₂O + K₂O), A/NK = Al_2O_3 /(Na₂O + K₂O), Fe* = FeOt/(FeOt + MgO) and Al (*agpaitic index* = molar proportion (Na + K)/Al.)

<dl: concentrations below detection limit; x: median.

ALK: Alkaline; CALCKP: Porphyritic High-K Calc-Alkaline.

and FeOt contents (1.7 – 5.3%, in which t denotes total Fe as FeO), and low MgO (< 0.9%) and TiO₂ (< 0.75%). Furthermore, these rocks are characterized by a relative high-field-strength elements (HFSE) and rare earth elements (REE) enrichment. Compositional variations among the granitic facies are related to decreasing alkalis, FeOt, CaO and Al₂O₃ contents from facies I to III (Table 1). Compared to the ALK and CALCKP suites, the CRB compositions differ from the CALKP suite especially on the alkalis, Ca, Mg, Fe (i.e., Fe* index = FeOt/FeOt + MgO; Frost et al., 2001) and HFSE abundances (Table 1). In this sense, the CRB approaches the compositions found in the ALK suite, as shown in Figures 4 and 5. Moreover, the batholith has metaluminous to slightly peraluminous character (A/CNK between 0.91 – 1.03 and A/NK 1.13 – 1.27), relative enrichment of light rare earth elements (LREE) over heavy rare earth elements (HREE) ($15.53 < \text{La}_{\text{N}}/\text{Yb}_{\text{N}} < 67.37$), moderate negative Eu anomalies ($0.58 < \text{Eu}/\text{Eu}^* < 1.64$, where $\text{Eu}^* = (\text{Gd}^*/\text{Yb})^{1/2}$), as well as negative Sr, P, Ti and Nb-Ta anomalies in chondrite-normalized spider diagrams (Figure 5). Nevertheless, the CRB chondrite-normalized REE patterns are distinct from most granite bodies in the ALK suite that show lower REE contents (especially the HREE) and positive Eu anomalies (cf. Nascimento et al., 2015 and references therein), except for the Flores stock (Souza et al., 2017) which is chemically very similar to the CRB.

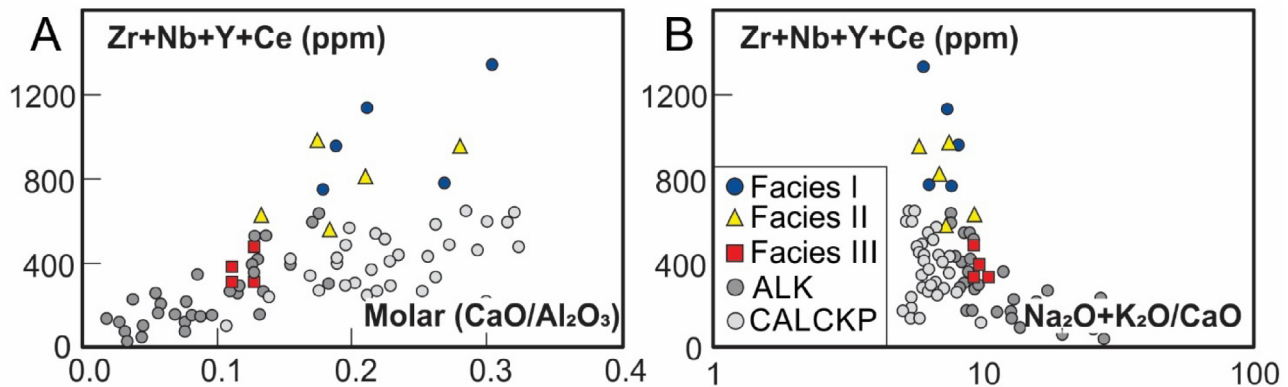
DISCUSSION

The Catolé do Rocha Batholith typology

Based on petrographical, structural and lithochemical criteria, Nascimento et al. (2015) have included the CRB in the CALCKP of the Ediacaran-Cambrian magmatism of the northern Borborema Province. The CALCKP suite

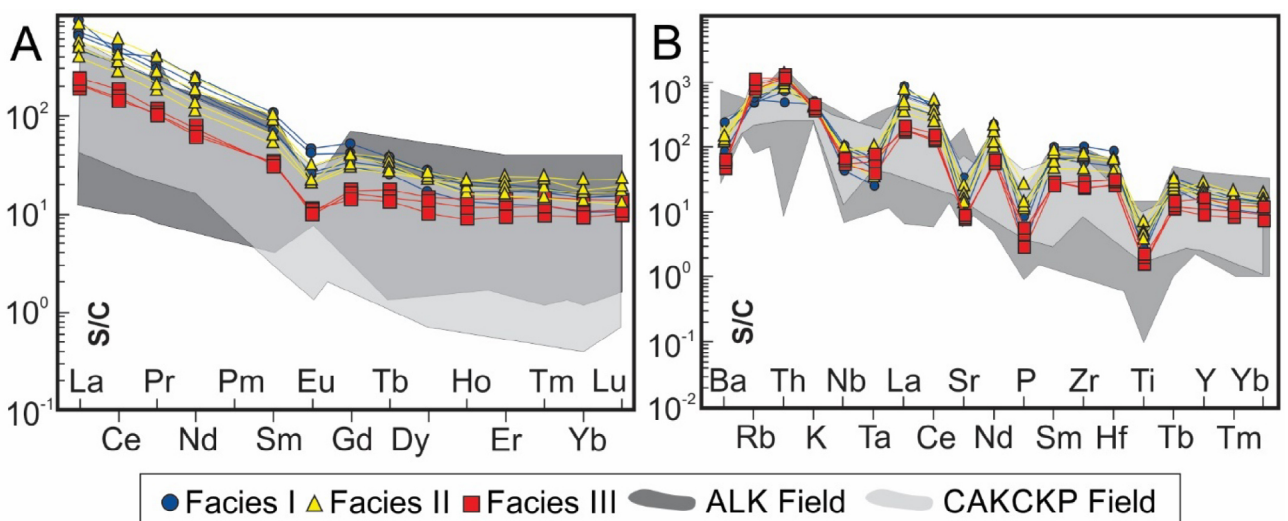
is composed mainly of monzogranite, monzonite, quartz monzonite and granodiorite (as well as dioritic enclaves) that follow calc-alkaline and subalkaline monzonite (or shoshonitic) magmatic trends (e.g., Lameyre, 1987; Nédélec and Bouchez, 2015) in the modal Q (quartz) — A (alkali feldspar) — P (plagioclase) diagram. Their compositions are transitional between calc-alkaline and alkaline, although many bodies, such as the Monte das Gameleiras and Barcelona plutons, have chemical signatures that are more calc-alkaline (*sensu* Rogers and Greenberg, 1981) and magnesian (*sensu* Frost et al., 2001; Figure 6A). According to the classification scheme of Frost et al. (2001; see also Frost and Frost, 2011; Castro, 2019), that relates granite types and magmatic series, the Fe* ratio (FeOt/FeOt + MgO wt %) is the best criterion (based on the major element composition) to distinguish between A- and I-type granites (whether they are Cordilleran or Caledonian; Pitcher, 1997; Chappell and Stephens, 1988). Therefore, A-type granites are characterized by higher Fe* ratios that yield typical ferroan signatures, whereas I-type granites (calc-alkalines) are characteristically magnesian (Figure 6A). This index is independent of alkali contents, as the latter are likely to increase with silica in most granite suites (e.g., King et al., 1997). However, considering the modified alkali-lime (MALI) index (Na₂O + K₂O-CaO) of Frost et al. (2001; Figure 6B), based on Peacock (1931) index series, A-type granites form mainly alkalic and alkali-calcic series, whereas I-type granites can belong to any of the Peacock series, from calcic to alkalic (Castro, 2019).

From the application of the granite typology concept, we noted that the CALCKP suite of Nascimento et al. (2015) encompasses mainly rocks with chemical signatures akin to Caledonian I-type granites *sensu* Pitcher (1983, 1997); i.e., post-collisional high-K calc-alkaline granites (although they also include some alkalic and alkali-calcic types), placed during crustal uplifting, extension and transcurrent tectonics (Figures 6A and 6B). In contrasts with the CALCKP



Source: modified from Whalen et al. (1987).

Figure 4. Lithochemical binary diagrams (major and trace elements). (A) $\text{CaO}/\text{Al}_2\text{O}_3$ versus $\text{Zr} + \text{Nb} + \text{Y} + \text{Ce}$. (B) $\text{Na}_2\text{O} + \text{K}_2\text{O}/\text{CaO}$ versus $\text{Zr} + \text{Nb} + \text{Y} + \text{Ce}$.



S/C: sample/chondrite.

Figure 5. Multi-element diagrams. (A) Rare-earth element patterns normalized to chondrite values of Boynton (1984). (B) Trace element spider diagram normalized to the chondrite values of Thompson (1982).

signature, the CRB has a notable ferroan composition and next to the alkalic and alkali-calcic series (besides the relative HFSE enrichment; Table 1; Figures 4 and 5), similar to the ALK suite of Nascimento et al. (2015; see also update in Dalan et al., 2019; Figures 6A and 6B). Some of these bodies are intrusive into the PSD, such as the Serra Negra do Norte pluton (Campos et al., 2000) and the Flores stock (Souza et al., 2017). Likewise, these rocks show alkaline signatures in several geochemical diagrams that are more typical of A-type granites (e.g., Whalen et al., 1987; King et al., 1997; Bonin, 2007). Additionally, the CRB shares petrographic, mineralogical, chemical and geochronological similarities with several A-type (transalkaline) granites from

the Alto Moxotó and Alto Pajeú terrains in the Transversal Zone Domain of the Borborema Province (e.g., plutons Queimadas and Pilóezinhos; Guimarães et al., 2004; Lima et al., 2017). The coexistence of A-type and Caledonian I-type (high-K calc-alkaline) granite suites is relatively common in post-collisional/extensional provinces such as the Death Valley region, USA (Calzia and Rämö, 2005) and the Itu Province, Southeast of Brazil (Janasi et al., 2009).

However, one has to recognize the drawbacks of using solely major elements to differentiate between calc-alkaline I-type and alkaline A-type granites. In fact, as pointed out by King et al. (1997), the concentration of “diagnostic” elements changes with the fractionation in both types, and the

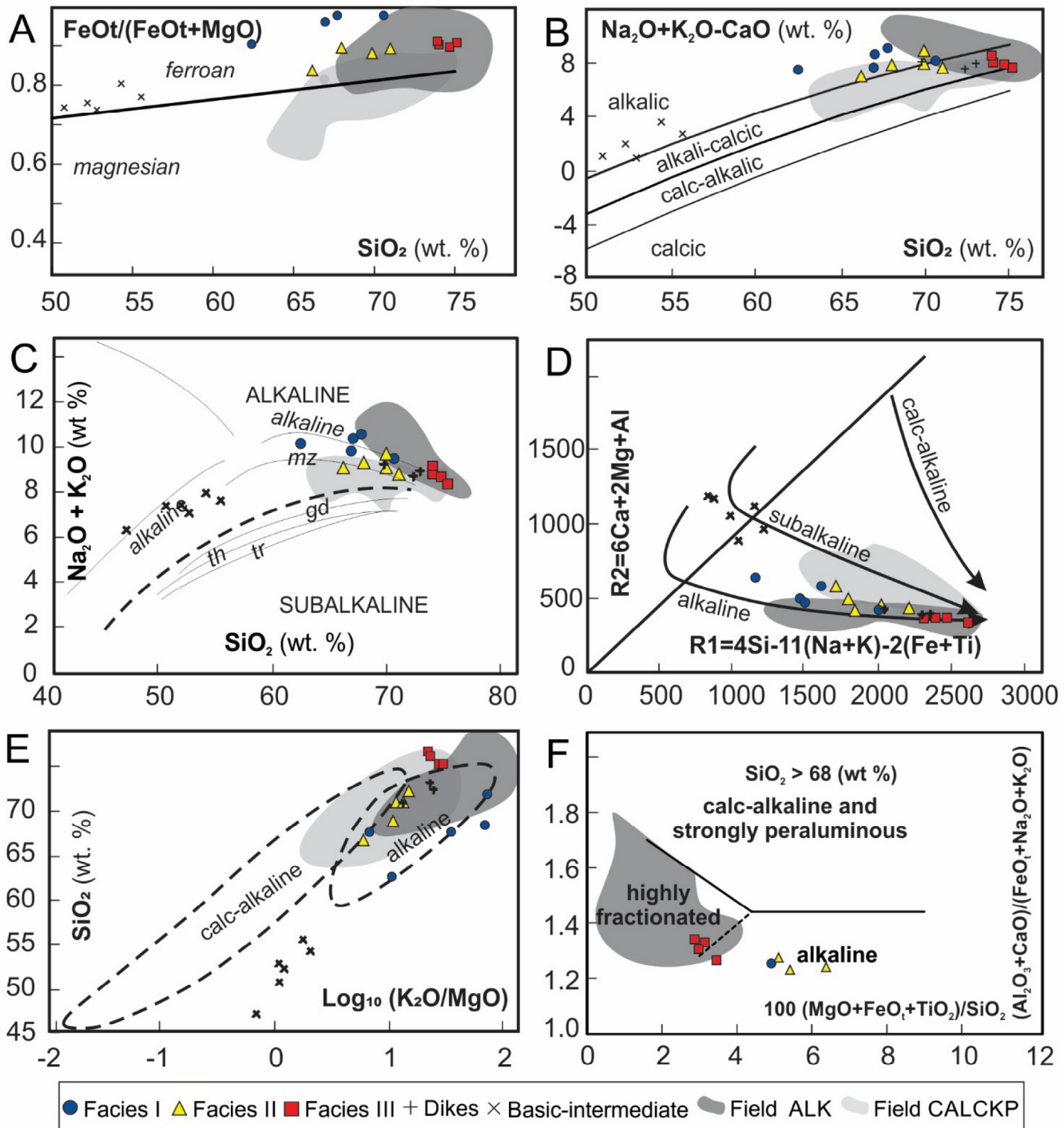


Figure 6. Magmatic series discriminant diagrams. (A) FeOt/(FeOt + MgO) (Fe index*) versus SiO₂ diagram of Frost et al. (2001). (B) Na₂O + K₂O-CaO (modified alkali-lime index – MALI) versus SiO₂ diagram of Frost et al. (2001). (C) Na₂O + K₂O versus SiO₂ diagram (Lameyre, 1987) with alkaline-subalkaline boundary after Middlemost (1985) and alkaline, monzonitic (mz), granodioritic (gd), trondhjemite (th) and tholeiitic (th) trends. (D) Cationic R1-R2 diagram (De La Roche, 1980). (E) SiO₂ versus log₁₀(K₂O/MgO) diagram of Rogers and Greenberg (1981). (F) Discriminant diagram (Al₂O₃ + CaO)/(FeOt + Na₂O + K₂O) versus 100*(MgO + FeOt + TiO₂)/SiO₂ for post-collisional granites with SiO₂ > 68 wt.% of Sylvester (1989). Data for granites from the Porphyritic High-K Calc-Alkaline and Alkaline suites of the ediacaran-cambrian magmatism in the Rio Piranhas-Seridó and São José do Campestre Domains were compiled from Campos et al. (2000), Nascimento et al. (2015) and Souza et al. (2017).

more evolved members of the calc-alkaline (= magnesian, I-type) series are prone to show the typical ferroan composition of the A-type granites (Frost et al., 2001; Frost and Frost, 2011; Castro, 2019). Castro (2019) proposed two scenarios for the magnesian to ferroan transition:

- magmatic differentiation under progressively more oxidizing conditions at the most evolved crystallization stages;
- as the result of changing either in the conditions of partial melting or the composition of the source areas, where a transition from I- to A-type granites is expected.

Conversely, King et al. (1997) stated that the typological classification of more evolved granites can be made with greater reliability from the composition of less evolved lithotypes of the same suite. In this sense, CRB granites are associated with basic-intermediate rocks which also have ferroan compositions (Figure 6A), whereas basic-intermediate rocks associated with CALCKP granites are predominantly magnesian (Jardim de Sá, 1994; Antunes et al., 2000; Nascimento et al., 2015). This observation corroborates the typological classification proposed here for the CRB.

The chemical contrasts among the CRB and other plutons in the CALCKP suite and its affinity with A-type granites were previously noted by Medeiros et al. (2008b) and Campos (2016). Moreover, based on hornblende and biotite mineral chemistry, Campos et al. (2016) concluded that the CRB belongs to the ilmenite series of Ishihara (1977) and crystallized under more reducing conditions, as opposed to the more oxidizing conditions for the CALCKP suite (magnetite series granites). To emphasize such contrasts, the CRB compositions were confronted with the CALCKP and ALK suites in several lithochemical diagrams (Figures 6 and 7).

The discrimination diagrams in Figure 6 clearly show the more alkaline character of the CRB in relation to the CALCKP suite. In particular, the total alkali vs. silica (Lameyre, 1987) and R1-R2 (De La Roche et al., 1980) plots (Figures 6C and 6D) allow distinguishing between the CALCKP suite, which follows a subalkaline trend (monzonite series in Figure 6C), and the ALK suite that plot along an alkaline trend, and how the latter overlaps with the CRB samples. Similarly, such contrasts also appear in the Sylvester (1989) diagram (Figure 6F), where the CRB shows alkaline affinity, whereas the CALCKP suite plots in the calc-alkaline field. Furthermore, the Sylvester's diagram also shows the affinity of the ALK suite with alkaline granites of similar compositions to highly fractionated I-type granites, which is consistent with the previous discussion.

To confirm the A-type affinity of CRB granites, we tested several granite typology classification diagrams (Figure 7). In those proposed by Whalen et al. (1987; Figures 7A and 7B), based on major element compositions, the agpaitic index ($\text{Na} + \text{K}/\text{Al}$, molar), and the Ga/Al ratio, CRB granites plot

mostly in the A-type field, in contrast to the CALCKP suite, which is more prone to the “non A-type” granites. Similarly, the CRB A-type signature is also confirmed in the diagrams of Whalen and Hildebrand (2019; Figure 7C) and Nardi and Bitencourt (2009; Figure 7D). They also reinforce the similarity that the CRB shares with the ALK suite and its contrasts with the CALCKP suite (“non A-type”; Figure 7D).

Eby (1992) divided the A-type granites into two varieties, namely A_1 -type and A_2 -type (see also Grebennikov, 2014). A_1 -type would be generated through fractionation of mantle-derived (OIB-like) magmas mainly during extensional regimes, while A_2 -type magmas may have originated by partial melting of mantle materials with crustal interaction or solely by the melting of crustal materials (lower crust), and were emplaced shortly after and orogenic period (post-collisional or post-orogenic environments). Therefore, the CRB granites classify as A_2 -type in the diagrams of Figures 7E and 7F.

Zircon trace elements

Zircon trace element composition has been used as a key in granite typological studies (e.g., Wang et al., 2012; Breiter et al., 2014; Sawaki et al., 2017). In A-type granites, zircon is characterized by relatively high Ce, Nb, Ta, U, Th, Hf and Y and low Sr and Eu contents, among other elements (Breiter et al., 2014; Sawaki et al., 2017). The analyzed CRB zircon ($n = 2$, facies I) register high Hf (up to 7,158 ppm), Y (up to 1634 ppm), Th (up to 214 ppm), and U (up to 120 ppm), and low Sr contents (0.4 ppm) (Figure 8A). Nb abundances are up to 2.6 ppm. The U/Th (~0.5–0.6) and Nb/Sr (~7.1) ratios are equivalent to those found in zircon crystals of A-type granites by Breiter et al. (2014) and Sawaki et al. (2017), respectively.

Chondrite-normalized rare-earth patterns for the CRB zircon are typical of igneous crystals (Hoskin and Ireland, 2000), being characterized by a relative enrichment of HREE over LREE ($1,664 < \text{Yb}_N/\text{La}_N < 1,730$ ppm), and positive and negative anomalies of Ce [$4.9 < \text{Ce}/\text{Ce}^* < 5.4$, where $\text{Ce}^* = (\text{La}_N \times \text{Pr}_N)^{1/2}$] and I [$0.16 < \text{Eu}/\text{Eu}^* < 0.2$, where $\text{Eu}^* = (\text{Sm}_N \times \text{Gd}_N)^{1/2}$] (Figure 8B).

Crystallization conditions

This section aims to refine the geothermobarometric estimates of Campos et al. (2016) for the CRB. Based on amphibole and biotite compositions (wavelength dispersive spectrometry (WDS) data) from facies I, these authors concluded that the CRB crystallized at pressures of $\sim 5.3 \pm 0.1$ kbar and temperatures of $732 \pm 8^\circ\text{C}$, under relatively low redox conditions ($\Delta_{\text{FO}_M} \sim -1.0$). Our new whole-rock analysis and mineral chemical data (EDS) for amphibole of facies I ($n = 3$, in which $n =$ number of analyzed crystals) and II ($n = 9$), and biotite of facies II ($n = 4$) and III ($n = 3$) (Table 2) allowed new and broad estimates of the intensive crystallization parameters

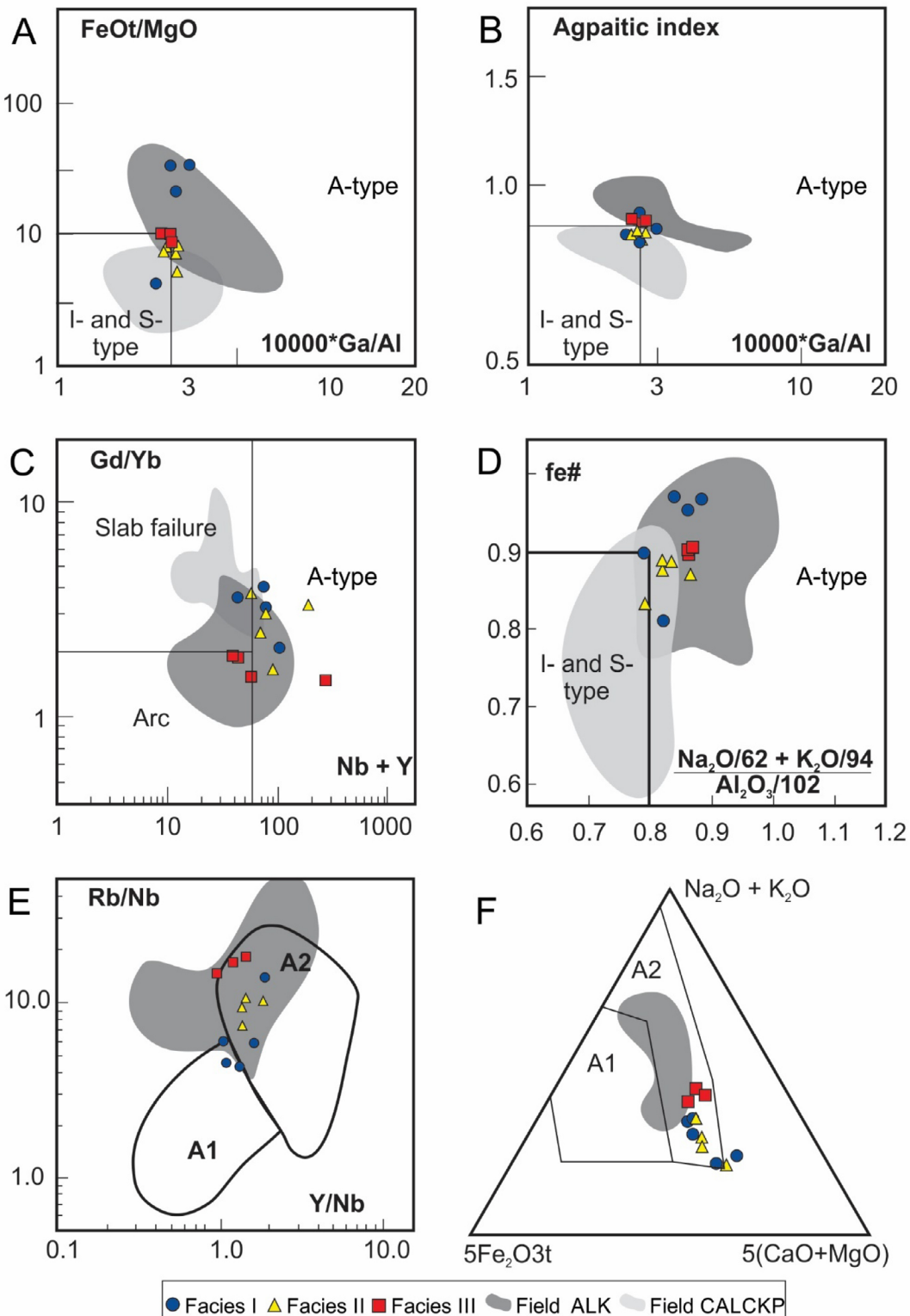


Figure 7. Granite typology discriminant diagrams. (A) $10000 \times \text{Ga}/\text{Al}$ versus FeO/MgO diagram of Whalen (1987). (B) $10000 \times \text{Ga}/\text{Al}$ versus agpaitic index ($\text{Na} + \text{K}/\text{Al}$, molar) of Whalen (1987). (C) $\text{Nb} + \text{Y}$ versus $\text{Gd} + \text{Yb}$ (ppm) diagram of Whalen and Hildebrand (2019). (D) Fe^* index ($\text{FeOt}/\text{FeOt} + \text{MgO}$, wt.%) versus alkalis/alumina ratio diagram of Nardi and Bitencourt (2009). (E) Yb/Nb versus Rb/Nb classification diagram for A-type granites of Eby (1992). (F) $5(\text{CaO} + \text{MgO})$ versus $\text{Na}_2\text{O} + \text{K}_2\text{O}$ versus $5\text{Fe}_2\text{O}_3\text{t}$ (wt.%) ternary discriminant diagram for A-type granites of Grebennikov (2014).

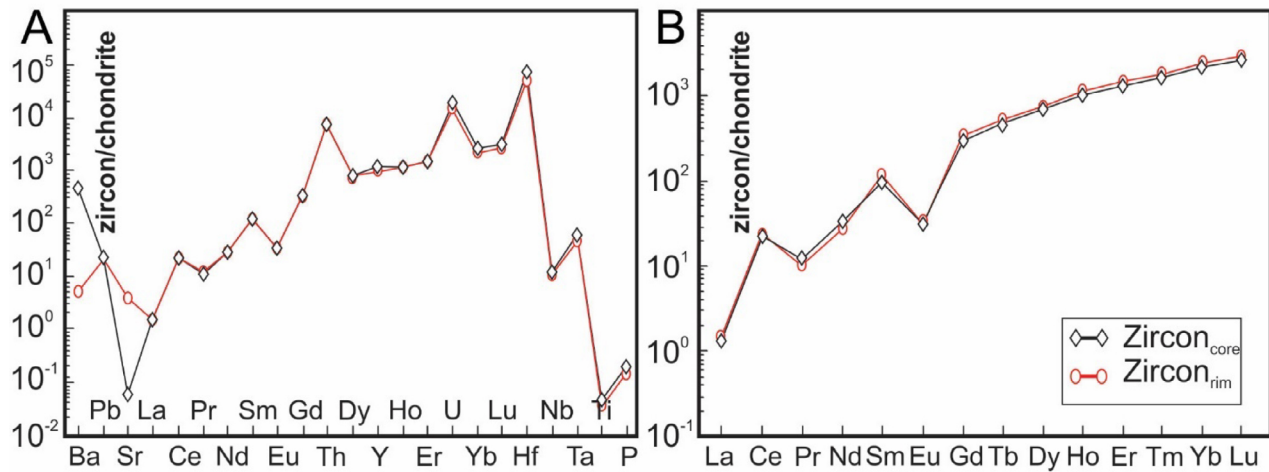


Figure 8. Multi-element diagrams for zircon in syenogranite of facies I. (A) Trace element spidergram normalized to the C1-chondrite values of McDonough and Sun (1995). (B) Rare-earth element patterns normalized to the C1-chondrite values of McDonough and Sun (1995).

Table 2. Chemical compositions (maximum, minimum and median values; wavelength dispersive spectrometry (WDS) and energy dispersive spectroscopy (EDS) analysis) for amphibole and biotite from the Catolé do Rocha Batholith. Cations per formula unit (cpfu) based on 13 total cations excluding Ca, Na and K (13eCNK) for amphibole and 22 oxygens for biotite.

Mineral	Amphibole				Biotite
	Facies	Syenogranite I	Syenogranite II	Syenogranite I	Syenogranite III
Samples (n)	3	9	4	3	
SiO ₂ (wt. %)	43.8 – 44.0 ($\bar{x} = 43.9$)	42.1 – 43.9 ($\bar{x} = 43.0$)	38.7 – 39.5 ($\bar{x} = 39.1$)	40.5 – 40.6 ($\bar{x} = 40.55$)	
TiO ₂	1.7 – 2.0 (1.85)	1.0 – 1.4 (1.2)	3.8 – 4.0 (3.9)	2.2 – 2.9 (2.55)	
Al ₂ O ₃	8.8 – 10.5 (9.65)	9.1 – 10.2 (9.65)	14.1 – 14.6 (14.35)	14.4 – 16.2 (15.3)	
FeOt	26.7 – 27.8 (27.25)	25.6 – 27.4 (26.5)	28.4 – 29.5 (28.95)	24.0 – 25.4 (24.7)	
MnO	0.5 – 0.6 (0.55)	0.5 – 0.8 (0.65)	< dl – 0.32 (0.16)	0.4 – 0.5 (0.45)	
MgO	3.3 – 3.5 (3.4)	5.0 – 6.0 (5.5)	4.1 – 4.4 (4.25)	6.9 – 7.2 (7.05)	
CaO	9.9 – 10.3 (10.1)	10.8 – 11.4 (11.1)	< dl	< dl	
Na ₂ O	1.9 – 2.1 (2.0)	1.3 – 1.6 (1.45)	< dl	< dl	
K ₂ O	1.4 – 1.5 (1.45)	1.3 – 1.7 (1.5)	9.1 – 9.5 (9.3)	9.4 – 9.8 (9.6)	
Si (cpfu)	6.68 – 6.76 (6.72)	6.40 – 6.64 (6.52)	5.85 – 5.94 (5.9)	5.95 – 5.99 (5.97)	
Al	1.60 – 1.88 (1.74)	1.62 – 1.82 (1.72)	2.51 – 2.59 (2.55)	2.52 – 2.79 (2.65)	
Ti	0.19 – 0.23 (0.21)	0.11 – 0.16 (0.135)	0.43 – 0.46 (0.44)	0.24 – 0.32 (0.28)	
Fe ³⁺	0.18 – 0.22 (0.2)	0.44 – 0.94 (0.69)	< dl	< dl	
Fe ²⁺	3.2 – 3.4 (3.3)	2.5 – 2.8 (2.65)	3.57 – 3.74 (3.65)	2.95 – 3.14 (3.05)	
Mn	0.07 – 0.08 (0.07)	0.07 – 0.10 (0.085)	dl – 0.04 (0.02)	< dl – 0.06 (0.03)	
Mg	0.75 – 0.8 (0.77)	1.15 – 1.34 (1.245)	0.91 – 0.98 (0.945)	1.52 – 1.59 (1.55)	
Ca	1.62 – 1.69 (1.65)	1.75 – 1.86 (1.81)	< dl	< dl	
Na	0.56 – 0.61 (0.58)	0.39 – 0.47 (0.43)	< dl	< dl	
K	0.27 – 0.30 (0.28)	0.25 – 0.33 (0.29)	1.73 – 1.83 (1.78)	1.78 – 1.83 (1.81)	
Fe(Fe + Mg)	0.81 – 0.82 (0.81)	0.71 – 0.75 (0.73)	0.79 – 0.80 (0.79)	0.65 – 0.67 (0.66)	

< dl = concentrations below detection limit. \bar{x} = median.

(P, T, f_{O_2}) using the geothermobarometers and oxibarometers listed in Table 3, along with the respective results.

Pressure

The calibrations of Schmidt (1992) and Ague (1997) for the Al-in-hornblende geobarometer were used for crystallization pressure estimates, based on our new hornblende chemical data (Table 2). Results indicate pressures between 4.3 – 6.0 kbar for facies I and 4.3 – 5.6 kbar for facies II (Table 3). These values, along with those from Campos et al. (2016), yield an average crystallization pressure of 5.1 ± 0.5 kbar for the CRB, which is consistent with the Ediacaran metamorphic peak in the region (3.8 – 5.7 kbar; Souza et al., 2007).

Temperature

For a better overview of the crystallization thermal interval, the following geothermometers were used: zircon saturation (TSatZrn; Watson and Harrison, 1983), apatite saturation (TSatAp; Harrison and Watson, 1984), liquid-only (Tliquid-only; Molina et al., 2015), Ti-in-zircon (TTizrn; Ferry and Watson, 2007), and Zr-in-titanite (TZrttn; Hayden and Watson, 2007). These thermometers have yielded higher temperature estimates that are likely to represent $T_{liquidus}$. Estimates of the $T_{solidus}$ were made with the amphibole-only geothermometer of Ridolfi et al. (2010).

The saturation geothermometers (zircon and apatite) returned values between 785 and 983°C (Table 3). TsatZr temperatures vary around 785 – 918°C (Figure 9) and increase from facies III to I. These values are in the range of temperatures

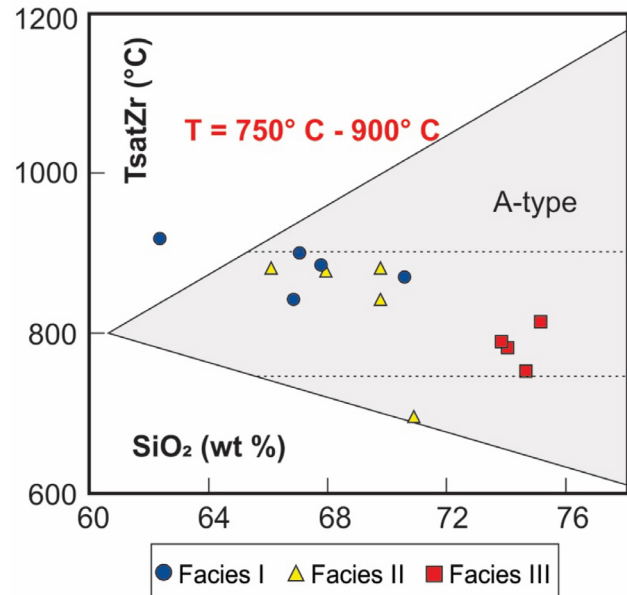


Figure 9. Zircon saturation temperature (TsatZr) versus SiO₂ diagram (symbols as in Figure 4). Gray field is the temperature interval for A-type granites after Eby (2011).

Table 3. Intensive crystallization parameters (P, T, f_{O_2}) for the Catolé do Rocha Batholith. Geothermobarometers and oxibarometers references are: S92 – Schmidt (1992); AS95 – Anderson and Smith (1995); A97 – Ague (1997); WH83 – Watson and Harrison (1983); HW84 – Harrison and Watson (1984); HB94 – Holland and Blundy (1994); FW07 – Ferry and Watson (2007); HW08 – Hayden and Watson (2007); R10 – Ridolfi et al. (2010); M15 – Molina et al. (2015); W81 – Wones (1981); SB15 – Smythe and Brenan (2015).

Facies	Syenogranite I	Syenogranite II	Syenogranite III	Campos et al. (2016)
Pressure estimates				
P_{S92} (kbar)	4.6 – 6.0	4.7 – 5.7	–	6.1 – 6.3
P_{AS95} (kbar)	–	–	–	5.2 – 5.6
P_{A97} (kbar)	4.3 – 5.3	4.3 – 5.1	–	5.4 – 5.5*
Temperature estimates				
T_{SatZrn}_{WH83} (°C)	870 – 918	839 – 880	785 – 810	874
T_{SatAp}_{HW84} (°C)	799 – 914	902 – 983	832 – 904	–
T_{HB94} (°C)	–	–	–	723 – 739
T_{Tizrn}_{FW07} (°C)	827 – 840	–	–	–
T_{Zrttn}_{H08} (°C)	684 – 702	–	–	–
T_{Amf}_{R10} (°C)	773 – 835	803 – 831	–	–
$T_{Liquidus}_{M15}$ (°C)	740 – 940	889 – 945	859 – 888	–
Oxygen fugacity estimates				
ΔFQM_{W81}	–	–	–	-1
Oxibarometer _{R10}	-15	-14	–	–
Oxibarometer	-18	–	–	–
$Ce-in-zircon_{SB15}(\log fO_2)$	–	–	–	–

*PA97 values obtained from data from Campos et al. (2016).

commonly found in A-type granites (~750 – 900°C; cf. Clemens et al., 1986; Patiño-Douce, 1997; King et al., 2001; Guimarães et al., 2004; Eby, 2011; Dalan et al., 2019) and agree well with the estimate of Campos et al. (2016) for the CRB (874°C; Table 3). The TsatAp geothermometer yielded temperatures between 799 and 983°C. These estimates overlap with TsatZrn temperatures, in agreement with the early magmatic precipitation of apatite and zircon in the studied rocks. Additionally, *Tliquidus* estimates with the liquid-only geothermometer of Molina et al. (2015) range from 740 to 945°C and are slightly lower in facies I (Table 3).

The Ti-in-zircon geothermometer (TTizrn; Watson and Harrison, 2005; Ferry and Watson, 2007) considers the $a\text{SiO}_2$ and $a\text{TiO}_2$ at the time of zircon crystallization, according to the Equation 1:

$$T(\text{°C}) = (-4800/(\log(T_{\text{zircon}}) + \log(a\text{SiO}_2) - \log(a\text{TiO}_2) - 5.711)) - 273 \quad (1)$$

In which:

T_{zircon} = Ti content (ppm) in zircon).

Calculations considered Ti contents measured in the zircon from facies I (15.6 – 17.4 ppm; cf. zircon trace elements section), with $a\text{SiO}_2$ and $a\text{TiO}_2$ fixed at 1.0 and 0.7 (Claiborne et al., 2010), respectively. Calculated temperatures vary between 827 and 840°C (Table 3), and are consistent with TsatZr estimates. Likewise, the Zr-in-titanite (TZrttn) geothermometer of Hayden et al. (2008) calculates the magma temperature at the time of titanite crystallization, according to the Equation 2:

$$T(\text{°C}) = [7708 + 960P]/[10.52 - \log(a\text{SiO}_2) - \log(a\text{TiO}_2) - \log(Z_{\text{titanite}})] - 273 \quad (2)$$

In which:

P = pressure (GPa);

Z_{titanite} = content of Zr (ppm) in titanite.

Values for $a\text{SiO}_2$ and $a\text{TiO}_2$ are the same used in TTizrn and the pressure was fixed at 5.5 kbar, as calculated with the Al-in-hornblende calibration of Ague (1997) for the titanite host-sample. Zr contents in a titanite crystal from facies I measured by LA-ICP-MS lie between 118 and 171 ppm, yielding Zr-in-titanite temperatures around 684 – 702°C (Table 3).

Finally, amphibole crystallization temperatures in facies I and II, calculated with the amphibole-only geothermometer of Ridolfi et al. (2010), vary between 773 – 835°C and 803 – 831°C, respectively, and are close to the values obtained by Campos et al. (2016) for facies I with the hornblende-plagioclase thermometry (723 – 739°C; Table 3).

Oxygen fugacity

The CRB granites crystallized under relatively reducing conditions ($\Delta_{\text{FO}_2} \sim -1.0$; Campos et al. (2016)), as opposed to the more oxidizing conditions of the CALCKP suite. Therefore, the batholith is made of reduced A₂-type granites, as confirmed by the binary diagram $\text{Al}_2\text{O}_3/(\text{K}_2\text{O}/\text{Na}_2\text{O})$ vs. $\text{FeO}(\text{FeO} + \text{MgO})$ (Dall'Agnol and Oliveira, 2007) of Figure 10A.

The reduced nature of the CRB granites is also supported by the composition of their mafic minerals. Values for fe# ($\text{Fe}/(\text{Fe} + \text{Mg})$) ratio are relatively high in amphibole (0.71 – 0.94) and biotite (0.65 – 0.92) (see also Campos et al., 2016), and these are consistent with low to intermediate $f\text{O}_2$ (Hollister et al., 1987; Anderson and Smith, 1995; Anderson, 1996; Figure 10B). In particular, based on the biotite fe# values, granites from facies I classify as “ilmenite-series granites”, while those of facies III, with slightly higher $f\text{O}_2$, belong to the “magnetite-series granites” of Anderson et al. (2008) (Figure 10C). Of note, titanomagnetite is the main Fe-Ti oxide in facies III. Dall'Agnol and Oliveira (2007) argued that magnetite crystallization can occur under high Fe# conditions, nevertheless the magma remains reduced. Hence, the presence of magnetite in granites is not incompatible with a more reduced character of its parental magmas (Anderson and Smith, 1995; Dall'Agnol and Oliveira, 2007; Anderson et al., 2008; Cunha et al., 2016; Campos et al., 2016).

We used the Ce-in-zircon oxybarometer (Ballard et al., 2002; Smythe and Brenan, 2015) in order to obtain more accurate $f\text{O}_2$ estimates. The method quantifies the magma $f\text{O}_2$ during zircon crystallization from the $\text{Ce}^{4+}/\text{Ce}^{3+}$ partition between zircon and liquid using the lattice strain model (Blundy and Wood, 1994). The Ce-in-zircon oxybarometer calibration of Smythe and Brenan (2015) considers the $a\text{SiO}_2$ and $a\text{TiO}_2$ of the magma at the time of zircon crystallization and these were fixed at 1.0 and 0.7, respectively, as for the TTizrn and TZrttn thermometric calculations. Results point to $\log_{f\text{O}_2}$ around -18 ($\Delta_{\text{FO}_2} \sim -4$) for temperatures between 840 and 827°C (obtained with the TTizrn thermometer; Figure 10D; Table 3). These conditions are compatible with the IW (iron-wüstite) and WM (wüstite-magnetite) buffers and corroborate reducing conditions during zircon crystallization in facies I (Figure 9D). Conversely, $\log_{f\text{O}_2}$ estimates based on amphibole composition (cf. Ridolfi et al., 2010) are between -15.8 and -14.2 ($-2.4 < \Delta_{\text{FO}_2} < -0.8$; Figure 9D). Such difference from zircon estimates may suggest, at least for facies I, magma crystallization under progressively more oxidizing conditions, since zircon is an early-crystallizing phase and hornblende appears at lower temperatures.

Magmatic differentiation

Based on the geochemical signatures and the behavior of major and trace elements in Harker-type variation diagrams

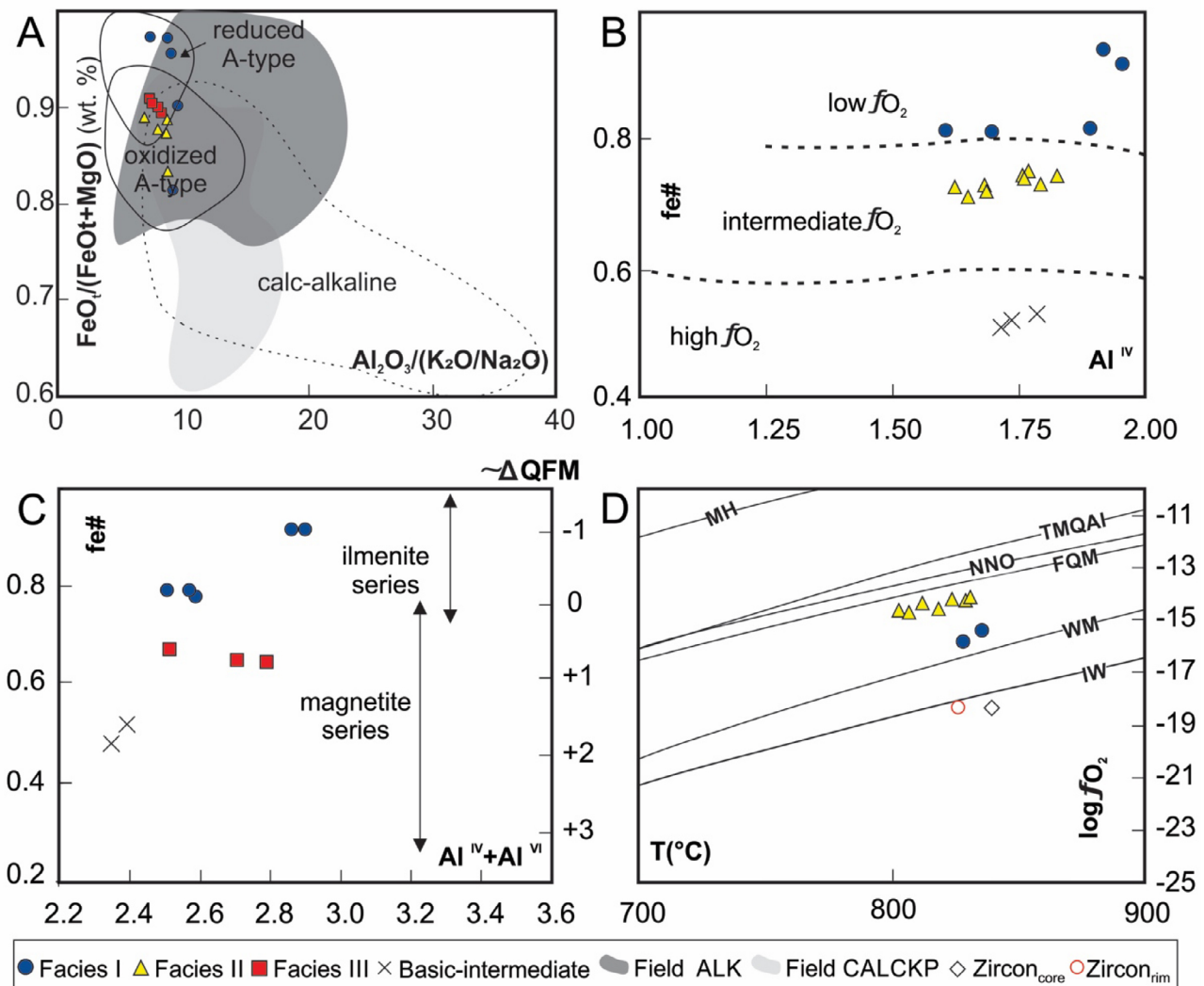


Figure 10. Estimates of redox crystallization conditions. (A) Binary $\text{Al}_2\text{O}_3/(\text{K}_2\text{O}+\text{Na}_2\text{O})$ versus $\text{FeO}_t/(\text{FeO}_t + \text{MgO})$ discriminant plot for reduced and oxidized A-type granites after Dall'Agnol and Oliveira (2007). (B) Al^{IV} versus $\text{fe}^{\#}$ [(Fe/(Fe + Mg))] (cations per formula unit – cpfu) plot for amphibole, with fields of low, intermediate and high $f\text{O}_2$ conditions according to Anderson and Smith (1995). (C) $\text{Al}^{\text{IV}} + \text{Al}^{\text{VI}}$ versus $\text{Fe}^{\#}$ (cpfu) plot for biotite after Anderson et al. (2008), compared to Laurentia Mesoproterozoic ilmenite-series and magnetite-series granite, with $f\text{O}_2$ relative to the FQM (fayalite-quartz-magnetite) buffer ($P_{\text{H}_2\text{O}} = P_{\text{total}}$) based on the calibration of Wones (1981). (D) $\log f\text{O}_2$ versus crystallization temperature calculated from amphibole (Ridolfi et al., 2010) and zircon (Smythe and Brenan, 2015) compositions for syenogranite from facies I and II. Buffers for P~6.0 kbar calculated from O'Neill (1988): IW: iron-wüstite; WM: wüstite-magnetite; FQM: quartz-fayalite-magnetite; NNO: nickel-bunsenite; TMQAI: titanite-magnetite-quartz-amphibole-ilmenite; MH: magnetite-ilmenite. Compositions of the mafic-intermediate rocks are plotted for comparison.

(Figure 11), it is likely that the CRB granites, basic-intermediate rocks and microgranite dykes do not share the same differentiation pathway, which rules out the hypothesis that these are cogenetic rocks (Medeiros et al., 2008b). In fact, it is possible to recognize two distinct trajectories for the felsic and basic-intermediate rocks in the Harker diagrams, and the existence of a possible compositional gap around $\text{SiO}_2 \sim 60$ wt.% (Figure 11). Moreover, the contrasting redox

conditions inferred for granites and basic-intermediate rocks (Figures 10B and 10C) reinforce that they may represent distinct magma batches.

The behavior of incompatible and compatible trace elements in bi-logarithmic diagrams can be used as a key to determine the main (or the latest) magmatic differentiation mechanism that shaped the geochemical characteristics of a given rock suite (e.g., Cocherie, 1986; Janoušek et al., 2006).

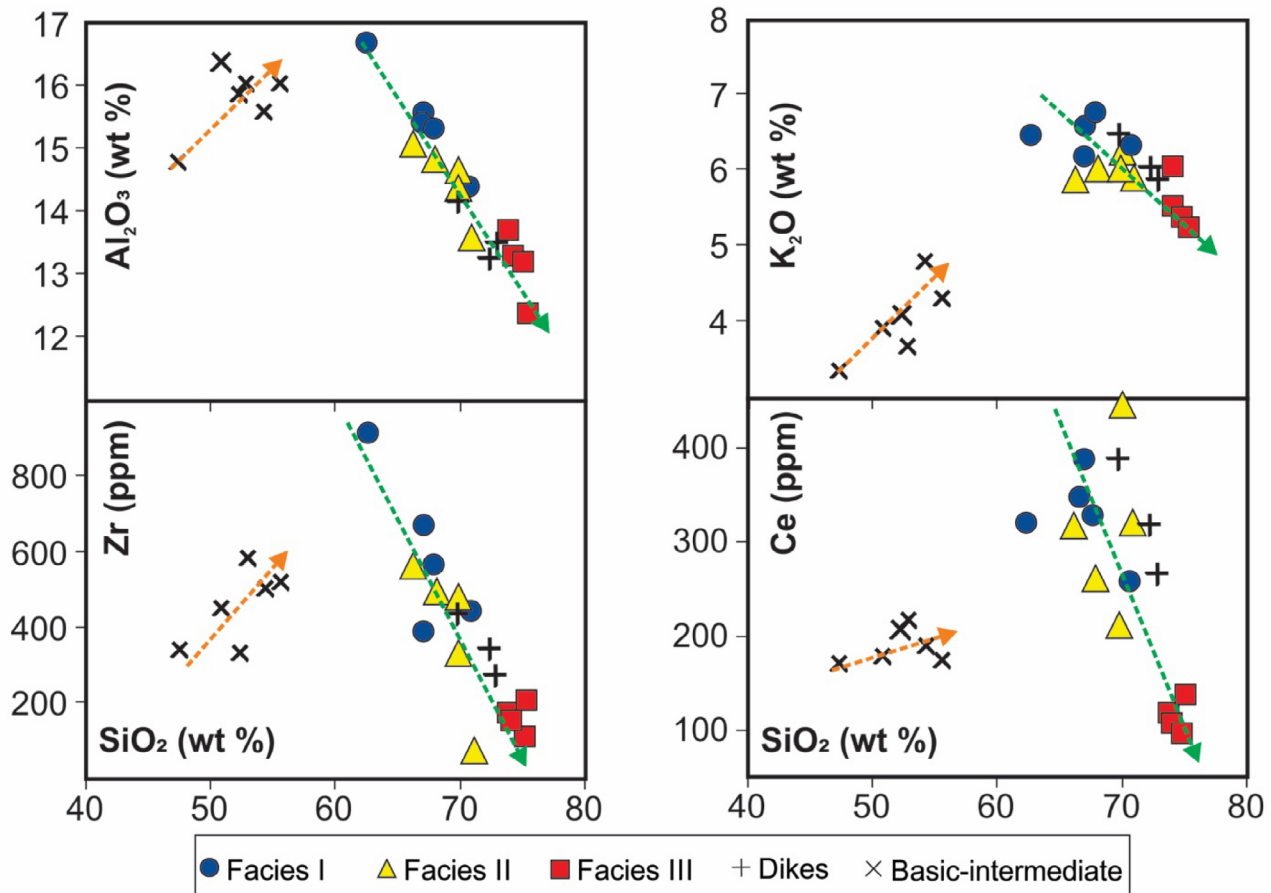
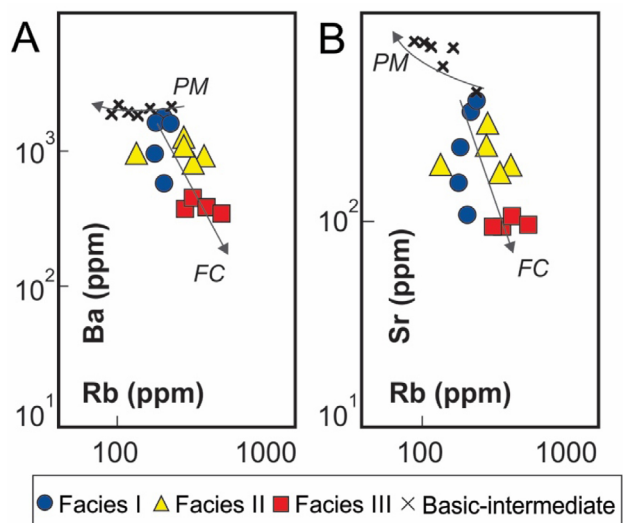


Figure 11. Harker-type plots (SiO_2 , wt% as differentiation index) for selected major and trace elements. Dashed lines are the interpreted differentiation trends for the granites (orange) and mafic-intermediate rocks (green).

In the bi-logs diagrams of Figures 12A and 12B, the almost vertical trend of negative slope observed for the granite samples suggests fractional crystallization as the dominant process for these rocks. Conversely, the basic-intermediate rocks plot along a nearly horizontal trend, which points to differentiation by partial melting of enriched sources (Janoušek et al., 2006). There is not enough geochemical evidence of magmas mixing processes in the CRB. However, due to the presence of schlierens, as well as rounded-shaped microgranular mafic enclaves that eventually show hybridization with the host syenogranites, at least locally the occurrence of mixing and/or mingling between granitic and basic-intermediate magmas cannot be ruled out.

The role of fractional crystallization is also supported by petrographic evidence (e.g., concentric zoning in plagioclase) and by the pronounced Ti, P and Sr negative anomalies in the spider diagram of Figure 5, suggesting ilmenite, apatite and plagioclase and/or hornblende fractionation. An attempt to relate by fractional crystallization the least evolved granite composition in the data set (sample VC634, facies I; Medeiros et al., 2008b) to the most evolved (daughter liquid)



FC: fractional crystallization; PM: partial melting.

Figure 12. Log(incompatible) versus log(compatible) plots. (A) Rb versus Ba, and (B) Rb versus Sr showing that the granites evolved by fractional crystallization, whereas mafic-intermediate rocks define a partial melting trend.

composition (sample VC641, facies III; Medeiros et al., 2008b) was made through major element least-square, mass-balance modeling with the spreadsheet PetroMode (Christiansen, 2009). The result in Table 4 shows that it is possible to generate a daughter liquid (C_{L_1}) with composition close to sample VC641 (C_{L_1}) after ~69% total crystallization of the parental sample VC634 (C_{L_0}) ($\sum r^2 = 0.079$). Fractionated minerals are orthoclase (47%), Fe-biotite (10%), plagioclase (bytownite, 5%), Fe-hornblende (3%), clinopyroxene (2.5%), titanite (0.8%), apatite (0.5%) and magnetite (0.2%) (Table 4).

Table 4. Major element least-square mass-balance geochemical modeling for the Catolé do Rocha granites.

Liquid composition	$C_{L_0} = \text{VC634}$ Facies III	$C_{L_1} = \text{VC641}$ Facies I	C_{L_1}	Cumulate minerals
SiO_2	62.73	75.48	75.48	Or (46.9%)
TiO_2	0.67	0.23	0.23	Bt (9.8%)
Al_2O_3	16.73	12.50	12.5	Pl (4.9%)
$\text{Fe}_2\text{O}_3\text{t}$	5.92	2.37	2.37	Hbl (3.3%)
MnO	0.09	0.03	0.03	Cpx (2.5%)
MgO	0.61	0.23	0.23	Ttn (0.8%)
CaO	2.79	0.77	0.77	Ap (0.5%)
Na_2O	3.76	3.10	3.10	Mt (0.2%)
K_2O	6.49	5.23	5.23	
P_2O_5	0.21	0.06	0.06	

CRB: Catolé do Rocha Batholith; Or: orthoclase; Bt: Fe-biotite; Pl: plagioclase (bytownite); Hbl: Fe-hornblende; Cpx: clinopyroxene; Ttn: titanite; Ap: apatite; Mt: magnetite.

Petrogenetic and geotectonic inferences

There are three major petrogenetic models for the generation of A-type granites:

- fractionation of mantle-derived (basaltic) magmas (Eby, 1990; Turner et al., 1992);
- partial melting of (lower) crustal sources (Collins et al., 1982; Patiño-Douce, 1997; Whalen et al., 1987);
- mixing between mantle-derived mafic magmas and crustal melts (Yang et al., 2006).

Recently, the generation of A-type magmas through partial melting of either metasomatized lower crust or lithospheric mantle has been invoked by many authors (e.g., Jiang et al., 2018; Vilalva et al., 2019). Furthermore, the required high *liquidus* temperatures to form these magmas suggest the involvement of mantle-derived melts, crustal delamination and mantle resurgence, especially in post-collisional environments (Kay and Kay, 1993; Lustrino, 2005).

Regardless of the petrogenetic model, A-type magma generation appears to be mainly associated with post-collisional and/or anorogenic environments (cf. for instance, Bonin, 2007; Nédélec and Bouchez, 2015). This is also true for the compositions of the CRB that plots within the post-collisional and intraplate fields in the tectonic discrimination diagrams of Pearce (1996) and Pearce et al. (1984) (Figures 13A and 13B). A post-collisional setting is consistent with its emplacement at 571 ± 3 Ma (zircon U/Pb; Medeiros et al., 2007) when the Rio Piranhas block was deforming by transtension. In fact, based on granite fabric patterns and anisotropy of magnetic

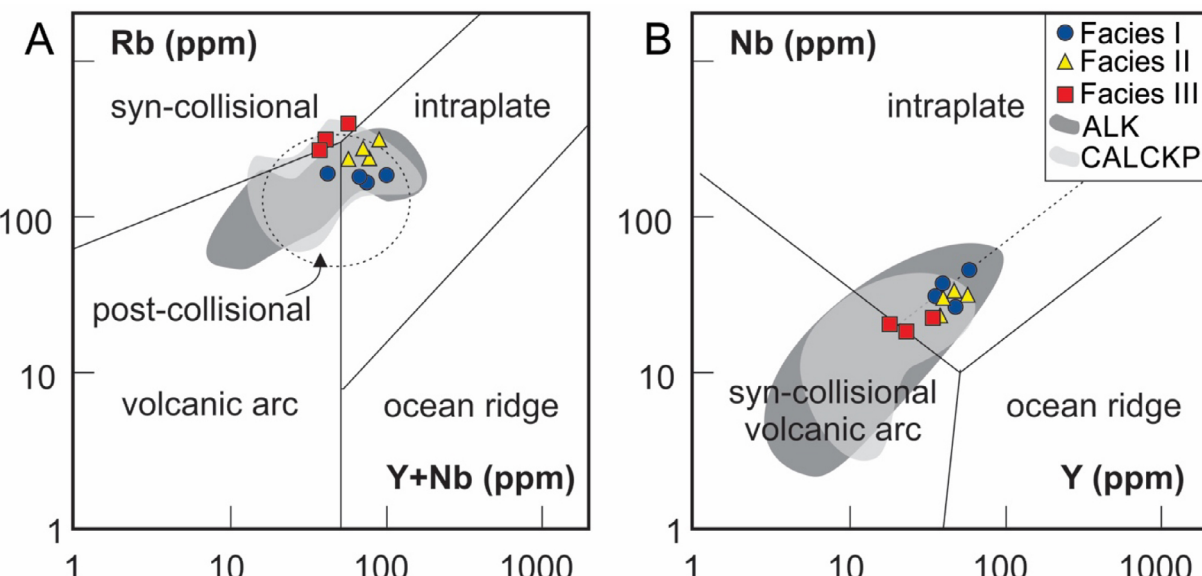


Figure 13. Trace element tectonic discrimination plots. (A) $\text{Y}+\text{Nb}$ versus Rb plot (ppm) of Pearce (1996). (B) Y versus Nb plot (ppm) of Pearce et al. (1984).

susceptibility studies, Archanjo et al. (1998, 2002) proposed a transcurrent/extensional environment for the emplacement of Ediacaran plutons located to the north of the CRB, in agreement with our geochemical results (see also Caby et al., 1991; Jardim de Sá, 1994; Vauchez et al., 1995; Archanjo et al., 1994).

Based solely on the available lithochemical data, we rule out the hypothesis of generation of CRB rocks through fractionation of mantle-derived magmas. In addition, CRB A₂-type granites contrast with the Caledonian I-type granites of the CALCKP suite by having higher Fe* ratio values, and REE, large-ion lithophile element (LILE) and HFSE (Zr, Nb, Y) abundances (Figures 4, 6, and 7). According to Eby (1992), A₂-type magmas have geochemical affinities to island arc basalts (IAB), suggesting derivation from sources previously modified (i.e., metasomatized) by slab-derived fluids from previous subducted materials, either the lithospheric mantle or the overlying lower continental crust, in post-collisional (or anorogenic) setting. Martin (2006) also argued that alkali- and silica-bearing fluids related to mantle upwelling in extensional environments can metasomatize the lower crust by fenitization type reactions. Based on geochemical data, Medeiros et al. (2008b) also suggest metasomatized mantle and deep crustal sources for the CRB mafic-c-intermediate and felsic magmas, respectively (Figure 14).

Lastly, the studied granites have relatively high contents of K, Th and U (Table 1) and can be classified as high heat-producing granites (cf. Rybach, 1988; Bea, 2012), with radiogenic heat production (*A*) between 2.3 and 5.3 μWm^{-3} (calculated after Rybach, 1988). These values are much higher

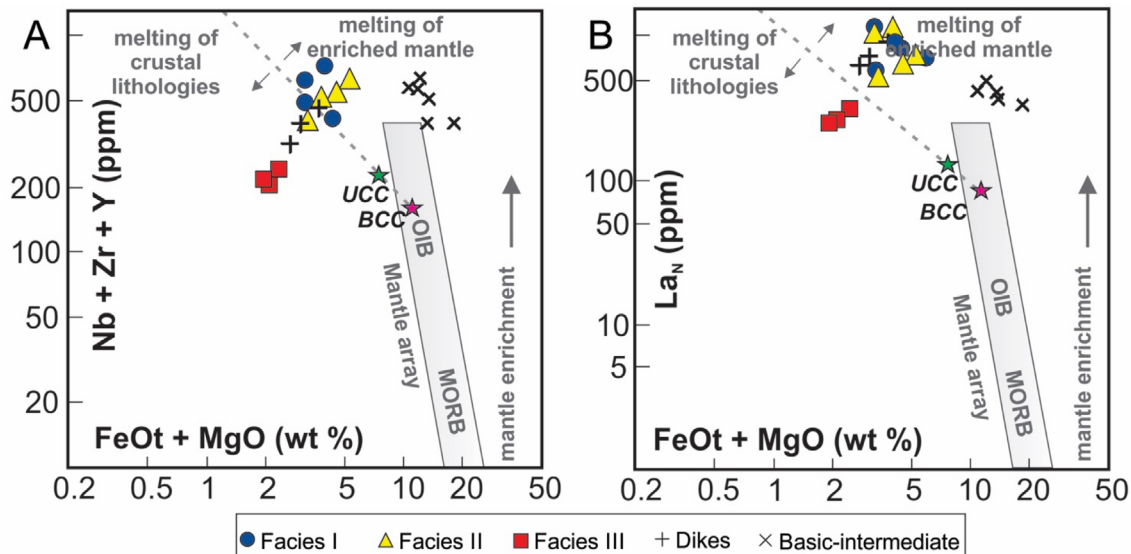
than average continental crust (1.0 – 1.2 μWm^{-3} ; Bea, 2012) and should reflect the enrichment of heat-producing elements (K, Th, U) in the source-areas due to metasomatic reactions driven by the circulation of alkaline fluids (Figures 14A and 14B; Martin, 2006; Bea, 2012; Vilalva et al., 2019).

In summary, the CRB granites have chemical characteristics that suggest the derivation of their magmas from enriched (metasomatized) sources, with evolution controlled by fractional crystallization, under low oxygen fugacities. Further isotopic studies are needed to better characterize the involved sources and magmatic processes.

CONCLUDING REMARKS

The CRB is one of the largest representants of the Ediacaran plutonism in the northernmost portion of the Borborema Province. This batholith is formed mainly by syenogranite and quartz syenite grouped in three distinct facies, microgranite and basic-intermediate rocks.

The granites are non-cogenetic with the basic-intermediate rocks and have relatively high alkali and low CaO and MgO contents, high FeOt/MgO ratios (ferroan granites), and significant concentrations of HFSE and REE. Similarly, their mafic silicates consist of Fe-enriched hornblende and biotite. These chemical features distinguish the batholith from most of the high-K calc-alkaline (subalkaline) bodies, and make it more akin to the alkaline granites. Therefore, we link the CRB to the A₂-type granites and suggest that it must to be



UCC: upper continental crust; BCC: bulk continental crust (Rudnick and Gao, 2003); MORB: mid-ocean ridge basalts; OIB: ocean island basalts.

Figure 14. Source discrimination plots of Laurent et al. (2014). (A) Incompatible Nb + Zr + Y (ppm) versus FeOt + MgO (wt.%) plot; (B) La concentrations normalized to C1-chondrite value of McDonough and Sun (1995) versus FeOt + MgO (wt. %) plot. Dashed line separating compositions of magmas derived from crustal- and enriched mantle sources is qualitatively represented by the “intracrustal” differentiation trend, i.e. the line joining upper- and bulk crustal compositions.

included in the Alkaline Suite of the Ediacaran-Cambrian magmatism in northern Borborema Province.

The granites crystallized at pressures between 4.6 and 6.3 kbar (\sim 16 – 24 km deep), at a temperature interval of ca. 950 – 750°C, and in a relatively reduced environment ($-4 < \Delta_{QFM} < -1$), therefore akin to reduced A₂-type granites (*sensu* Dall'Agnol and Oliveira, 2007). The magma would result from partial melting of a metasomatized source (either the lithospheric mantle or the overlying lower crust) generated the felsic melts, with further differentiation by fractional crystallization processes. The coexistence with non-cogenetic mafic-intermediate magmas is evidenced by schlierens and microgranular mafic enclaves that locally show hybridization with the host granite. Whether these basic-intermediate magmas originate from the partial melting of metasomatized lithospheric mantle and were the heat source for melting the overlying metasomatized lower crust that ultimately generated the batholith, remains an open question for future studies.

ACKNOWLEDGEMENTS

The authors thank the financial and academical support from the Programa de Pós-Graduação em Geodinâmica e Geofísica-UFRN (PPGG/UFRN), and the analytical support from the Núcleo de Apoio à Pesquisa Geoanalítica-USP and Laboratório de Caracterização de Minerais/Materiais (LACAMM)-IFRN. The authors also acknowledge two anonymous reviewers for their comments and suggestions that helped improve the original manuscript, and the journal's editorial staff.

REFERENCES

- Ague, J. J. (1997). Thermodynamic calculation of emplacement pressures for batholithic rocks, California: implications for the aluminum-in-hornblende barometer. *Geology*, 25(6), 563-566. [https://doi.org/10.1130/0091-7613\(1997\)025<0563:TCOE>2.3.CO;2](https://doi.org/10.1130/0091-7613(1997)025<0563:TCOE>2.3.CO;2)
- Almeida, F. F. M., Hasui, Y., Brito Neves, B. B., Fuck, R. A. (1981). Brazilian structural provinces: an introduction. *Earth- Science Reviews*, 17(1-2), 1-29. [https://doi.org/10.1016/0012-8252\(81\)90003-9](https://doi.org/10.1016/0012-8252(81)90003-9)
- Anderson, J. L. (1996). Status of thermobarometry in granitic batholiths. *Earth and Environmental Science Transactions of the Royal Society of Edinburgh*, 87(1-2), 125-138. <https://doi.org/10.1017/S0263593300006544>
- Anderson, J. L., Barth, A. P., Wooden, J. L., Mazdab, F. (2008). Thermometers and thermobarometers in granitic systems. *Reviews in Mineralogy and Geochemistry*, 69(1), 121-142. <https://doi.org/10.2138/rmg.2008.69.4>
- Anderson, J. L., Smith, D. R. (1995). The effect of temperatures and oxygen fugacity on Al-in-hornblende barometry. *American Mineralogist*, 80(5-6), 549-559. <https://doi.org/10.2138/am-1995-5-614>
- Angelim, L. A. A., Medeiros, V. C., Nesi, J. R. (2006). Programa Geologia do Brasil - PGB. Projeto Mapa Geológico e de Recursos Minerais do Estado do Rio Grande do Norte. *Mapa Geológico do Estado do Rio Grande do Norte*. Escala 1:500.000. Recife: CPRM/FAPERN. Available at: <http://www.cprm.gov.br/ppublico/media/geologia_basica/cartografiaRegional/mapa_rio_grande_norte.pdf>. Accessed on: Jan. 28, 2020.
- Antunes, A. F., Galindo, A. C., Alves da Silva, F. C., Jardim de Sá, E. F., Souza Lima, R. F. (2000). Magmatismo Granítico de afinidade Subalcalina/Monzonítica no Maciço São José de Campestre, Província Borborema (NE do Brasil): O exemplo do Plutônio de Monte das Gameleiras. *Geochimica Brasiliensis*, 14(1), 51-69. Available at: <<http://www.ppegeo.igc.usp.br/index.php/geobras/article/view/10483>>. Accessed on: Aug. 19, 2020.
- Archango, C. J., Bouchez, J. L., Corsini, M., Vauchez, A. (1994). The Pombal granite pluton: magnetic fabric, emplacement and relationships with the Brasiliense strike-slip setting of the NE Brazil (Paraíba State). *Journal of Structural Geology*, 16(3), 323-335. [https://doi.org/10.1016/0191-8141\(94\)90038-8](https://doi.org/10.1016/0191-8141(94)90038-8)
- Archango, C. J., Macedo, J. W. P., Galindo, A. C. X., Araújo, M. G. S. (1998). Brasiliano crustal extension and emplacement fabrics of the mangerite-charnockite pluton of Umarizal, Northeast Brazil. *Precambrian Research*, 87(1-2), 19-32. [https://doi.org/10.1016/S0301-9268\(97\)00050-8](https://doi.org/10.1016/S0301-9268(97)00050-8)
- Archango, C. J., Trindade, R. I. F., Bouchez, J. L., Ernesto, M. (2002). Granite fabrics and regional-scale strain partitioning in the Seridó belt (Borborema Province, NE Brazil). *Tectonics*, 21(1), 3-1-3-14. <https://doi.org/10.1029/2000TC001269>
- Archango, C. J., Viegas, L. G. F., Hollanda, M. H. B. M., Souza, L. C., Liu, D. (2013). Timing of the HT/LP transgression in the Neoproterozoic Seridó Belt (Borborema Province, Brazil): constraints from U/Pb (SHRIMP) geochronology and implications for the connections between NE Brazil and West Africa. *Gondwana Research*, 23(2), 701-714. <https://doi.org/10.1016/j.gr.2012.05.005>
- Ballard, J. R., Palin, J. M., Campbell, I. H. (2002). Relative oxidation states of magmas inferred from Ce(IV)/Ce(III) in zircon: application to porphyry copper deposits of northern Chile. *Contributions to Mineralogy and Petrology*, 144, 347-364. <https://doi.org/10.1007/s00410-002-0402-5>

- Bea, F. (2012). The sources of energy for crustal melting and the geochemistry of heatproducing elements. *Lithos*, 153, 278-291. <https://doi.org/10.1016/j.lithos.2012.01.017>
- Blundy J., Wood B. (1994). Prediction of crystal-melt partition coefficients from elastic moduli. *Nature*, 372, 452-454. <https://doi.org/10.1038/372452a0>
- Bonin, B. (2007). A-type granites and related rocks: Evolution of a concept, problems and prospects. *Lithos*, 97(1-2), 1-29. <https://doi.org/10.1016/j.lithos.2006.12.007>
- Boynton, W. V. (1984). Geochemistry of the rare earth elements: meteorite studies. In: P. Henderson, P. (Ed.). *Rare Earth Element Geochemistry*. Amsterdam: Elsevier, v. 2, p. 63-114. <https://doi.org/10.1016/B978-0-444-42148-7.50008-3>
- Breiter, K., Lamarão, C. N., Borges, R. M. K., Dall'Agnol, R. (2014). Chemical characteristic of zircon from A-type granites and comparison to zircon of S-type granites. *Lithos*, 192-195, 208-225. <https://doi.org/10.1016/j.lithos.2014.02.004>
- Brito Neves, B. B, Santos, E. D., Van Schmus, W. R. (2000). Tectonic history of the Borborema Province. In: U. Cordani, E. J. Milani, A. Thomaz Filho, D. A. Campos (Eds.). *Tectonic Evolution of South America* (p. 151-182). Rio de Janeiro: 31st International Geological Congress Special Publication.
- Caby, R., Sial, A. N., Arthaud, M. H., Vauchez, A. (1991). Crustal Evolution and the Brasiliano Orogeny in Northeast Brazil. In: R. D. Dallmeyer, J. P. Lecorche (Eds.). *The West African Orogens and Circum-Atlantic Correlatives* (p. 373-397). Berlin: Springer-Verlag. https://doi.org/10.1007/978-3-642-84153-8_16
- Calzia, J. P., Rämö, O. T. (2005). Miocene rapakivi granites in the southern Death Valley region, California, USA. *Earth-Science Reviews*, 73(1-4), 221-243. <https://doi.org/10.1016/j.earscirev.2005.07.006>
- Campos, B. C. S. (2016). *Petrografia, litoquímica, química mineral e termobarometria de rochas cálculoalcalinas de alto K de textura porfirítica, ediacaranas, no extremo NE da Província Borborema (NE do Brasil)*. MSc Dissertation. Natal: Programa de Pós-Graduação em Geodinâmica e Geofísica, Universidade Federal do Rio Grande do Norte. Available at: <<https://repositorio.ufrn.br/jspui/handle/123456789/21307>>. Accessed on: Jan. 20. 2020.
- Campos, C. S. C., Vilalva, F. C. J., Nascimento, M. A., Galindo, A. C. (2016). Crystallization conditions of porphyritic high-K calc-alkaline granitoids in the extreme northeastern Borborema Province, NE Brazil, and geodynamic implications. *Journal of South American Earth Sciences*, 70, 224-236. <https://doi.org/10.1016/j.jsames.2016.05.010>
- Campos, T. F. C., Neiva, A. M. R., Nardi, L. S. V. (2000). Geochemistry of granites and their minerals from Serra Negra do Norte Pluton, northeastern Brazil. *Chemie der Erde*, 60(4), 279-303.
- Castro, A. (2019). The dual origin of I-type granites: The contribution from laboratory experiments. *Geological Society Special Publications*, 491, 101-145. <https://doi.org/10.1144/SP491-2018-110>
- Chappell, B. W., Stephens, W. E. (1988). Origin of infracrustal (I-type) granite magmas. *Transactions of the Royal Society of Edinburgh: Earth Sciences*, 79(2-3), 71-86. <https://doi.org/10.1017/S0263593300014139>
- Christiansen, E. H. (2009). *PetroMode*. Faculty Publications, 1334. Brigham: Brigham Young University. Available at: <<https://scholarsarchive.byu.edu/facpub/1334>>. Accessed on: Aug. 19, 2020.
- Claiborne, L. L., Miller, C. F., Wooden, J. L. (2010). Trace element composition of igneous zircon: a thermal and compositional record of the accumulation and evolution of a large silicic batholith, Spirit Mountain, Nevada. *Contributions to Mineralogy and Petrology*, 160(4), 511-531. <https://doi.org/10.1007/s00410-010-0491-5>
- Clemens, J. D., Holloway, J. R., White, A. J. R. (1986). Origin of an A-type granite: experimental constraints. *American Mineralogist*, 71(3-4), 317-324.
- Cocherie, A. (1986). Systematic use of trace element distribution patterns in log-log diagrams for plutonic suites. *Geochimica et Cosmochimica Acta*, 50(11), 2517-2522. [https://doi.org/10.1016/0016-7037\(86\)90034-7](https://doi.org/10.1016/0016-7037(86)90034-7)
- Collins, W. J., Beams, S. D., White, A. J. R., Chappell, B. W. (1982). Nature and origin of A-type granites with particular reference to southeastern Australia. *Contributions to Mineralogy and Petrology*, 80, 189-200. <https://doi.org/10.1007/BF00374895>
- Cunha, A. L. C., Costa, A. P., Cavalcante, R., Dantas, A. R. (2018). *Projeto ARIM Seridó – Folha Catolé do Rocha SB.24-Z-A-III, Estados da Paraíba e do Rio Grande do Norte*. Carta geológica-Geofísica. 1 mapa colorido, 90,00 cm x 75,00 cm. Escala 1:100.000. Avaliação dos Recursos Minerais do Brasil. Recife: CPRM – Serviço Geológico do Brasil. Available at: <<http://rigeo.cprm.gov.br/jspui/handle/doc/18668>>. Accessed on: Jan. 28, 2020.

- Cunha, I. R. V., Dall'Agnol, R., Feio, G. R. L. (2016). Mineral chemistry and magnetic petrology of the Archean Planalto Suite, Carajás Province–Amazonian Craton: Implications for the evolution of ferroan Archean granites. *Journal of South American Earth Sciences*, 67, 100-121. <https://doi.org/10.1016/j.jsames.2016.01.007>
- Dalan, C. A., Vilalva, F. C. J., Nascimento, M. A. L. (2019). Reavaliação das condições de cristalização de granitos alcalinos ediacaranos dos domínios Rio Piranhas-Seridó e São José do Campestre, Província Borborema, NE-Brasil. *Geologia USP. Série Científica*, 19(1), 129-152. <https://doi.org/10.11606/issn.2316-9095.v19-149112>
- Dall'Agnol, R., Oliveira, D. C. (2007). Oxidized, magnetiteseries, rapakivi-type granites of Carajás, Brazil: implications for classification and petrogenesis of A-type granites. *Lithos*, 93(3-4), 215-233. <https://doi.org/10.1016/j.lithos.2006.03.065>
- De La Roche, H., Leterrier, J., Granclaude, P., Marchal, M. (1980). A classification of volcanic and plutonic rocks using R1-R2 diagram and major element analyses. Its relationship with current nomenclature. *Chemical Geology*, 29(1-4), 183-210. [https://doi.org/10.1016/0009-2541\(80\)90020-0](https://doi.org/10.1016/0009-2541(80)90020-0)
- Eby, G. N. (1990). The A-type granitoids a review of their occurrence and chemical characteristics and speculations their petrogenesis. *Lithos*, 26(1-2), 115-134. [https://doi.org/10.1016/0024-4937\(90\)90043-Z](https://doi.org/10.1016/0024-4937(90)90043-Z)
- Eby, G. N. (1992). Chemical subdivision of the A-type granitoids: petrogenetic and tectonic implications. *Geology*, 20(7), 641-644. [https://doi.org/10.1130/0091-7613\(1992\)020<0641:CSOTA>2.3.CO;2](https://doi.org/10.1130/0091-7613(1992)020<0641:CSOTA>2.3.CO;2)
- Eby, G. N. (2011). A-type granites: magma sources and their contribution to the growth of the continental crust. 7th *Hutton Symposium on Granites and Related Rocks*. Avila, Spain.
- Ferreira, A. C., Dantas, E. L., Fuck, R. A., Nedel, I. M. (2020). Arc accretion and crustal reworking from late Archean to Neoproterozoic in Northeast Brazil. *Scientific Reports*, 10(1), 7855. <https://doi.org/10.1038/s41598-020-64688-9>
- Ferry, J. M., Watson, E. B. (2007). New thermodynamic models and revised calibrations for the Ti-in-zircon and Zr-in-rutile thermometers. *Contributions to Mineralogy and Petrology*, 154, 429-437. <https://doi.org/10.1007/s00410-007-0201-0>
- Frost, B. R., Barnes, C. G., Collins, W. J., Arculus, R. J., Ellis, D. J., Frost, C. D. (2001). A geochemical classification for granitic rocks. *Journal of Petrology*, 42(11), 2033-2048. <https://doi.org/10.1093/petrology/42.11.2033>
- Frost, C. D., Frost, B. R. (2011). On ferroan (A-type) granitoids: their compositional variability and modes of origin. *Journal of Petrology*, 52(1), 39-53. <https://doi.org/10.1093/petrology/egq070>
- Gonçalves, L. C. (2009). *Contribuição geofísica a análise do arcabouço tectônico do Domínio Rio Grande do Norte, Província Borborema – NE Brasil*. Dissertation (Mastering). Brasília: Instituto de Geociências, Universidade de Brasília. Available at <<https://core.ac.uk/download/pdf/33540762.pdf>>. Accessed on: Aug. 19, 2020.
- Grebennikov, A. V. (2014). A-type granites and related rocks: petrogenesis and classification. *Russian Geology and Geophysics*, 55(11), 1354-1356. <https://doi.org/10.1016/j.rgg.2014.10.011>
- Griffin, W. L., Powell, W. J., Pearson, N. J., O'Reilly, S. Y. (2008). GLITTER: data reduction software for laser ablation ICP-MS. In: P. Sylvester (Ed.). *Laser Ablation ICP-MS in the Earth Sciences: Current practices and outstanding issues* (v. 40, p. 307-311). Vancouver: Mineralogical Association of Canada.
- Guimarães, I. P., Silva Filho, A. F., Almeida, C. N., Van Schmus, W. R., Araújo, J. M., Melo, S. C., Melo, E. B. (2004). Brasiliano (Pan-African) granitic magmatism in the Pajeú-Paraíba belt, Northeast Brazil: an isotopic and geochronological approach. *Precambrian Research*, 135(1-2), 23-53. <https://doi.org/10.1016/j.precamres.2004.07.004>
- Harrison, T. M., Watson, E. B. (1984). The behavior of apatite during crustal anatexis: equilibrium and kinetic considerations. *Geochimica et Cosmochimica Acta*, 48(7), 1467-1477. [https://doi.org/10.1016/0016-7037\(84\)90403-4](https://doi.org/10.1016/0016-7037(84)90403-4)
- Hayden, L. A., Watson, E. B. (2007). Rutile saturation in hydrous siliceous melts and its bearing on Ti-thermometry of quartz and zircon. *Earth and Planetary Science Letters*, 258(3-4), 561-568. <https://doi.org/10.1016/j.epsl.2007.04.020>
- Hayden, L. A., Watson, E. B., Wark, D. A. (2008). A thermobarometer for sphene (titanite). *Contributions to Mineralogy and Petrology*, 155, 529-540. <https://doi.org/10.1007/s00410-007-0256-y>
- Holland, T., Blundy, J. (1994). Non-ideal interactions in calcic amphiboles and their bearing on amphibole-plagioclase thermometry. *Contributions to Mineralogy and Petrology*, 116(4), 433-447. <https://doi.org/10.1007/BF00310910>
- Hollanda, M. H. B., Archanjo, C. J., Souza, L. C., Dunyi, L., Armstrong, R. (2011). Long-lived paleoproterozoic granitic magmatism in the Seridó-Jaguaribe domain, Borborema Province–NE Brazil. *Journal of South American Earth Sciences*, 32(4), 287-300. <https://doi.org/10.1016/j.jsames.2011.02.008>

- Hollister, L. S., Grissom, G. C., Peters, E. K., Stowell, H. H., Sisson, V. B. (1987). Confirmation of the empirical correlation of Al in hornblende with pressure of solidification of calc-alkaline plutons. *American Mineralogist*, 72(3-4), 231-239.
- Hoskin, P. W. O., Ireland, T. R. (2000). Rare earth element chemistry of zircon and its use as a provenance indicator. *Geology*, 28(7), 627-630. [https://doi.org/10.1130/0091-7613\(2000\)28%3C627:REECOZ%3E2.0.CO;2](https://doi.org/10.1130/0091-7613(2000)28%3C627:REECOZ%3E2.0.CO;2)
- Ishihara, S. (1977). The magnetite-series and ilmenite-series granitic rocks. *Mining Geology*, 27(145), 293-305. <https://doi.org/10.11456/shigenchishitsu1951.27.293>
- Janasi, V. A., Vlach, S. R. F., Campos Neto, M. C., Ulbrich, H. H. (2009). Associated A-type subalkaline and high-K calc-alkaline granites in the Itu granite province, southeastern Brazil: petrological and tectonic significance. *The Canadian Mineralogist*, 47(6), 1505-1526. <https://doi.org/10.3749/canmin.47.6.1505>
- Janoušek, V., Farrow, C. M., Erban, V. (2006). Interpretation of whole-rock geochemical data in igneous geochemistry: introducing Geochemical Data Toolkit (GCDkit). *Journal of Petrology*, 47(6), 1255-1259. <https://doi.org/10.1093/petrology/egl013>
- Jardim de Sá, E. F. (1994). *A Faixa Seridó (Província Borborema, NE do Brasil) e o seu significado geodinâmico na cadeia Brasiliiana/Pan-Africana*. Brasília. Thesis (Doctoring). Brasília: Programa de Pós-graduação em Geologia, Instituto de Geociências, Universidade de Brasília.
- Jardim de Sá, E. F., Macedo, M. H., Fuck, R. A., Kawashita, K. (1992). Terrenos proterozóicos na Província Borborema e a margem norte do Cráton São Francisco. *Brazilian Journal of Geology*, 22(4), 472-480.
- Jiang, X. Y., Ling, M. X., Wu, K., Zhang, Z. K., Sun, W. D., Sui, Q. L., Xia, X. P. (2018). Insights into the origin of coexisting A1-and A2-type granites: implications from zircon Hf-O isotopes of the Huayuangong intrusion in the lower Yangtze River Belt, eastern China. *Lithos*, 318-319, 230-243. <https://doi.org/10.1016/j.lithos.2018.08.008>
- Kay, R. W., Kay, S. M. (1993). Delamination and delamination magmatism. *Tectonophysics*, 219(1-3), 177-189. [https://doi.org/10.1016/0040-1951\(93\)90295-U](https://doi.org/10.1016/0040-1951(93)90295-U)
- King, P. L., Chappell, B. W., Allen, C. M., White, A. J. R. (2001). Are A-type granites the high-temperature felsic granites? Evidence from fractionated granites of the Wangrah Suite. *Australian Journal of Earth Sciences*, 48(4), 501-514. <https://doi.org/10.1046/j.1440-0952.2001.00881.x>
- King, P. L., White, A. J. R., Chappel, B. W., Allen, C. M. (1997). Characterization and origin of aluminous A-type granites from the Lachland fold belt, southeastern Australia. *Journal of Petrology*, 38(3), 371-391. <https://doi.org/10.1093/petroj/38.3.371>
- Lameyre, J. (1987). Granites and evolution of the crust. *Revista Brasileira de Geociências*, 17(4), 349-359. Available at: <<http://www.ppegeo.igc.usp.br/index.php/rbg/article/view/11926>>. Accessed on: Sept. 17, 2020.
- Laurent, O., Martin, H., Moyen, J.-F., Doucelance, R. (2014). The diversity and evolution of late-Archean granites: Evidence for the onset of a “modern-style” platetectonics between 3.0 and 2.5 Ga. *Lithos*, 205, 208-235. <https://doi.org/10.1016/j.lithos.2014.06.012>
- Lima, J. V., Guimarães, I. P., Santos, L., Amorim, J. V. A., Farias, D. J. S. (2017). Geochemical and isotopic characterization of the granitic magmatism along the Remígio-Pocinhos shear zone, Borborema Province, NE Brazil. *Journal of South American Earth Sciences*, 75, 116-133. <https://doi.org/10.1016/j.jsames.2017.02.004>
- Lustrino, M. (2005). How the delamination and detachment of lower crust can influence basaltic magmatism. *Earth-Science Reviews*, 72(1-2), 21-38. <https://doi.org/10.1016/j.earscirev.2005.03.004>
- Martin, R. F. (2006). A-type granites of crustal origin ultimately result from open-system fenitization-type reactions in an extensional environment. *Lithos*, 91(1-4), 125-136. <https://doi.org/10.1016/j.lithos.2006.03.012>
- McDonough, W. F., Sun, S. S. (1995). The composition of the Earth. *Chemical Geology*, 120(3-4), 223-253. [https://doi.org/10.1016/0009-2541\(94\)00140-4](https://doi.org/10.1016/0009-2541(94)00140-4)
- Medeiros, V. C., Amaral, C. A., Rocha, D. E. G. A., Santos, R. B. (2008a). *Geologia e Recursos Minerais da Folha Sousa SB.24-X-A*. Escala 1:250.000. Estados da Paraíba, Rio Grande do Norte e Ceará. Recife: CPRM – Serviço Geológico do Brasil. Available at <<http://rigeo.cprm.gov.br/jspui/handle/doc/10861>>. Accessed on: Jan. 28, 2020.
- Medeiros, V. C., Galindo, A. C., Nascimento, M. A. L. (2008b). Litogeochímica do Batólito de Catolé do Rocha (RN-PB), porção W do Domínio Rio Grande do Norte da Província Borborema. *Estudos Geológicos*, 18(1), 28-44. Available at: <<http://www3.ufpe.br/estudosgeologicos/>>. Accessed on: Aug. 19, 2020.

- Medeiros, V. C., Galindo, A. C., Nascimento, M. A. L., Freire, A. G. (2007). Geologia, petrografia e idade do Batólito de Catolé do Rocha (RN-PB), porção W do Domínio Rio Grande do Norte da Província Borborema. *Revista de Geologia*, 20, 219-230.
- Middlemost, E. A. K. (1985). *Magmas and Magmatic Rocks: An Introduction to Igneous Petrology*. London and New York: Longman. 266 p.
- Molina, J. F., Moreno, J. A., Castro, A., Rodríguez, C., Fershtater, G. B. (2015). Calcic amphibole thermobarometry in metamorphic and igneous rocks: new calibrations based on plagioclase/amphibole Al-Si partitioning and amphibole/liquid Mg partitioning. *Lithos*, 232, 286-305. <https://doi.org/10.1016/j.lithos.2015.06.027>
- Mori, P. E., Reeves, S., Correia, C. T., Haukka, M. (1999). Development of a fused glass disc XRF facility and comparison with the pressed powder pellet technique at Instituto de Geociências, São Paulo University. *Revista Brasileira de Geociências*, 29(3), 441-446. <https://doi.org/10.25249/0375-7536.199929441446>
- Nardi, L. V. S., Bitencourt, M. F. (2009). A-type granitic rocks in post-collisional settings in southernmost Brazil: their classification and relationship with tectonics and magmatic series. *Canadian Mineralogist*, 47(6), 1493-1503. <https://doi.org/10.3749/canmin.47.6.1493>
- Nascimento, M. A. L., Galindo, A. C., Medeiros, V. C. (2015). Ediacaran to Cambrian magmatic suites in the Rio Grande do Norte domain, extreme Northeastern Borborema Province (NE of Brazil): Current knowledge. *Journal of South American Earth Sciences*, 58, 281-299. <https://doi.org/10.1016/j.jsames.2014.09.008>
- Nascimento, M. A. L., Medeiros, V. C., Galindo, A. C. (2008). Magmatismo Ediacarano a Cambriano no Domínio Rio Grande do Norte, Província Borborema, NE do Brasil. *Estudos Geológicos*, 18(1), 4-29. Available at: <<http://www3.ufpe.br/estudosgeologicos/>>. Accessed on: Aug. 19, 2020.
- Nédélec, A., Bouchez, J. L. (2015). *Granites: petrology, structure, geological setting, and metallogeny*. Oxford Scholarship Online. <https://doi.org/10.1093/acprof:oso/9780198705611.001.0001>
- O'Neill, H. St. C. (1988). Systems Fe–O and Cu–O: thermodynamic data for the equilibria Fe–“FeO,” Fe– Fe_3O_4 , “FeO”– Fe_3O_4 , Fe_3O_4 – Fe_2O_3 , Cu– Cu_2O , and Cu_2O – CuO from emf measurements. *American Mineral*, 73, 470-486.
- Available at: <http://www.minsocam.org/msa/collectors_corner/amtoc/toc1988.htm>. Accessed on: Aug. 19, 2020.
- Patiño-Douce, A. (1997). Generation of metaluminous A-type granites by low pressure melting of calc-alkaline granitoids. *Geology*, 25(8), 743-746. [https://doi.org/10.1130/0091-7613\(1997\)025%3C0743:GOMATG%3E2.3.CO;2](https://doi.org/10.1130/0091-7613(1997)025%3C0743:GOMATG%3E2.3.CO;2)
- Peacock, M. A. (1931). Classification of igneous rock series. *The Journal of Geology*, 39(1), 54-67. <https://doi.org/10.1086/623788>
- Pearce, J. (1996). Sources and settings of granitic rocks. *Episodes*, 19(4), 120-125. <https://doi.org/10.18814/epiugs/1996/v19i4/005>
- Pearce, J. A., Harris, N. B., Tindle, A. G. (1984). Trace element discrimination diagrams for the tectonic interpretation of granitic rocks. *Journal of Petrology*, 25(4), 956-983. <https://doi.org/10.1093/petrology/25.4.956>
- Pitcher, W. S. (1983). Granite type and tectonic environment. *1st Symposium on Mountain Building*, 19-40. London: Academic Press.
- Pitcher, W. S. (1997). *The nature and origin of granite*. London: Chapman & Hall.
- Ridolfi, F., Renzulli, A., Puerini, M. (2010). Stability and chemical equilibrium of amphibole in calc-alkaline magmas: an overview, new thermobarometric formulations and application to subduction-related volcanoes. *Contributions to Mineralogy and Petrology*, 160(1), 45-66. <https://doi.org/10.1007/s00410-009-0465-7>
- Rogers, J. J. W., Greenberg, J. K. (1981). Trace elements in continental margin magmatism. Part III. Alkali granites and their relationship to cratonization. *Bulletin Geological Society of America*, 92(1), 6-9. [https://doi.org/10.1130/0016-7606\(1981\)92<6:TEICMP>2.0.CO;2](https://doi.org/10.1130/0016-7606(1981)92<6:TEICMP>2.0.CO;2)
- Rudnick, R. L., Gao, S. (2003). Composition of the continental crust. In: R. L. Rudnick (Ed.). *Treatise on geochemistry* (p. 1-64). Amsterdam: Elsevier.
- Rybäck, L. (1988). Determination of heat production rate. In: R. Haenel, L. Rybäck, L. Stegenga (Eds.). *Handbook of terrestrial-flow density determinations* (p. 125-142). Dordrecht: Kluwer Academic Publishers.
- Santos, E. J. (1996). Ensaio preliminar sobre terrenos e tectônica acrecional na Província Borborema. *Congresso Brasileiro de Geologia*, 39, 47-50. Salvador: SBG.

- Santos, E. J., Brito Neves, B. B., Van Schmus, W. R., Oliveira, R. G., Medeiros, V. C. (2000). An overall view on the displaced terrane arrangement of the Borborema Province, NE Brazil. *International Geological Congress*, 31, 5-9. Rio de Janeiro.
- Santos, L. D. L., Dantas, E. L., Cawood, P. A., Lages, G. D. A., Lima, H. M., Santos, E. J. (2018). Accretion Tectonics in Western Gondwana Deduced From Sm-Nd Isotope Mapping of Terranes in the Borborema Province, NE Brazil. *Tectonics*, 37(8), 2727-2743. <https://doi.org/10.1029/2018TC005130>
- Sawaki, Y., Suzuki, K., Asanuma, H., Okabayashi, S., Hattori, K., Saito, T., Hirata, T. (2017). Geochemical characteristics of zircons in the Ashizuri A-type granitoids: An additional granite topology tool for detrital zircon studies. *Island Arc*, 26(6), e12216. <https://doi.org/10.1111/iar.12216>
- Schmidt, M. W. (1992). Amphibole composition in tonalite as a function of pressure: an experimental calibration of the Al-in-hornblende barometer. *Contributions to Mineralogy and Petrology*, 110(2-3), 304-310. <https://doi.org/10.1007/BF00310745>
- Smythe, D. J., Brenan, J. M. (2015). Cerium oxidation state in silicate melts: combined fo_2 , temperature and compositional effects. *Geochemica et Cosmochimica Acta*, 170, 173-187. <https://doi.org/10.1016/j.gca.2015.07.016>
- Souza, V. O., Galindo, A. C., Alves da Silva, F. C. (2017). O Stock Flores: Exemplo de magmatismo granítico tipo-A no Domínio Rio Piranhas-Seridó, NE da Província Borborema. *Pesquisas em Geociências*, 44(2), 345-366. <https://doi.org/10.22456/1807-9806.78278>
- Souza, Z. S., Kalsbeek, F., Deng, X. D., Frei, R., Kokfelt, T.F., Dantas, E. L., Li, J. W., Pimentel, M. M., Galindo, A. C. (2016). Generation of continental crust in the northern part of the Borborema Province, northeastern Brazil, from Archaean to Neoproterozoic. *Journal of South American Earth Sciences*, 68, 68-96. <https://doi.org/10.1016/j.jsames.2015.10.006>
- Souza, Z. S., Martin, H., Peucat, J., Jardim de Sá, E. F., Macedo, M. H. F. (2007). Calc-Alkaline Magmatism at the Archean-Proterozoic Transition: the Caico Complex Basement (NE Brazil). *Journal of Petrology*, 48(11), 2149-2185. <https://doi.org/10.1093/petrology/egm055>
- Sylvester, P. J. (1989). Post-collisional alkaline granites. *Journal of Geology*, 97(3), 261-280. <https://doi.org/10.1086/629302>
- Thompson, R. N. (1982). Magmatism of the British Tertiary volcanic province. *Scottish Journal of Geology*, 18(1), 49-107. <https://doi.org/10.1144/sjg18010049>
- Turner, S. P., Foden, J. D., Morrison, R. S. (1992). Derivation of some A-type magmas by fractionation of basaltic magma: an example from the Padthaway Ridge, South Australia. *Lithos*, 28(2), 151-179. [https://doi.org/10.1016/0024-4937\(92\)90029-X](https://doi.org/10.1016/0024-4937(92)90029-X)
- Vauchez, A., Neves, S., Caby, R., Corsini, M., Egydio-Silva, M., Arthaud, M., Amaro, V. (1995). The Borborema shear zone system, NE Brazil. *Journal of South American Earth Sciences*, 8(3-4), 247-266. [https://doi.org/10.1016/0895-9811\(95\)00012-5](https://doi.org/10.1016/0895-9811(95)00012-5)
- Vilalva, F. C. J., Simonetti, A., Vlach, S. R. F. (2019). Insights on the origin of the Graciosa A-type granites and syenites (Southern Brazil) from zircon U-Pb geochronology, chemistry, and Hf and O isotope compositions. *Lithos*, 340-341, 20-33. <https://doi.org/10.1016/j.lithos.2019.05.001>
- Wang, Y., Wang, J., Wang, L., Long, L., Tang, P., Liao, Z., Zhang, H., Shi, Y. (2012). The Tuerkubantao Ophiolite Mélange in Xinjiang, NW China: New Evidence for the Erqis Suture Zone. *Geoscience Frontiers*, 3(5), 587-602. <https://doi.org/10.1016/j.gsf.2012.02.002>
- Watson, E. B., Harrison, T. M. (1983). Zircon saturation revisited: temperature and composition effects in a variety of crustal magma types. *Earth and Planetary Science Letters*, 64(2), 295-304. [https://doi.org/10.1016/0012-821X\(83\)90211-X](https://doi.org/10.1016/0012-821X(83)90211-X)
- Watson, E. B., Harrison, T. M. (2005). Zircon thermometer reveals minimum melting conditions on earliest. *Earth Science*, 308(5723), 841-844. <https://doi.org/10.1126/science.1110873>
- Whalen, J. B., Currie, K. L., Chappell, B. W. (1987). A-type granites: Geochemical characteristics, discrimination and petrogenesis. *Contributions to Mineralogy and Petrology*, 95, 407-419. <https://doi.org/10.1007/BF00402202>
- Whalen, J. B., Hildebrand, R. S. (2019). Trace element discrimination of arc, slab failure, and A-type granitic rocks. *Lithos*, 348-349, 105179. <https://doi.org/10.1016/j.lithos.2019.105179>
- Wones, D. R. (1981). Mafic silicates as indicators of intensive variables in granitic magmas. *Mining Geology*, 31(168), 191-212. <https://doi.org/10.11456/shigenchishitsu1951.31.191>
- Yang, J. H., Wu, F. Y., Chung, S. L., Wilde, S. A., Chu, M. F. (2006). A hybrid origin for the Qianshan A-type granite, Northeast China: geochemical and Sr-Nd-Hf isotopic evidence. *Lithos*, 89(1-2), 89-106. <https://doi.org/10.1016/j.lithos.2005.10.002>